according to the RA classification criteria of the American College of Rheumatology, published in 1987 (23) and in 2010 (24). All patients had shown inadequate responses to treatment with more than one conventional disease-modifying anti-rheumatic drug (DMARD), and were initiated with one of the four biologics as the first biologic, according to the guidelines of the Japan College of Rheumatology (25, 26). To follow up patients who moved to other hospitals, we sent an inquiry in May 2012 to their current physicians. We asked whether the patients were still on the same treatment, and if not, the reason for discontinuation.

Treatments

Biologics were administered according to the package insert drug information for Japan: TCZ, 8 mg/kg as a single intravenous drip infusion administered every 4 weeks; IFX, 3 mg/kg (loading dose up to 10 mg/kg was permitted in July 2009) as a single intravenous drip infusion administered at weeks 0, 2, 6, and every 8 weeks after week 6; ETN, 25 mg or 50 mg as a single subcutaneous injection administered 1 or 2 times a week; and ADA, 40 mg as a single subcutaneous injection administered every 2 weeks. Changes in doses of biologics and other drugs were not recorded in this study. Determination of efficacy, remission, and discontinuation of biologics was dependent on each doctor.

Outcomes

The primary end-point of this study was the duration of drug administration. Specific causes of drug discontinuation were also examined, and cause-specific relative hazards of discontinuation were calculated as the secondary outcome.

Variables

We assessed variables such as sex, age, disease duration, complications (diabetes and interstitial pneumonia, IP), concomitant dosage of methotrexate (MTX) and corticosteroid (equivalent to prednisolone, PRD), the Disease Activity Score in 28 joints based on the C-reactive protein levels as assessed by three variables [DAS28-CRP(3)], and DAS28 components (27) at the initiation of the biologics.

Statistical methods

Drug continuation rates of the biologics were examined using Kaplan–Meier estimates and were compared using the log-rank test. Cases discontinued due to remission or miscellaneous reasons and missing cases were treated as censored cases. Baseline characteristics of the patients are summarized as median (range), and differences between biologics were analysed using the Kruskal–Wallis non-parametric test for continuous variables and the χ^2 test for categorical variables. Cause-specific hazard ratios (HRs) for drug discontinuation were calculated using the Cox proportional hazard model, which was adjusted for variables such as age, DAS28, existence of diabetes or IP, and concomitant dosage of MTX and PRD. We selected variables for each multivariate analysis based on the results of univariate analysis, stepwise logistic regression analysis, and the clinical importance of each variable. All analyses were performed using JMP version 9.0 (SAS Institute Inc., Cary, NC, USA), and a p-value < 0.05 was considered statistically significant. In this study, we followed the Strengthening the Reporting of Observational Studies in Epidemiology (STROBE) statement for transparent reporting (28).

Results

Study population

Of the 401 patients included in this study, 348 received the first biologic at Osaka University Hospital and 53 patients received it at other hospitals. At the end of April 2012, 322 patients were being followed at our institute, and the other 72 patients were followed through inquiries. We confirmed the duration of drug administration and causes of discontinuation in 394 patients in April 2012. Thus, the missing seven patients and those still on therapy were handled as censored cases in the Kaplan–Meier curves (Supplementary Figure 1).

Patients

TCZ, IFX, ETN, and ADA were administered as the first biologic for the treatment of RA to 97, 103, 143, and 58 patients, respectively. Demographic characteristics of the patients differed between these treatment groups (Table 1). (Where patient data points are missing, the number of patients without missing values is given at each entry.) Statistically significant differences in age, DAS28, disease duration, and concomitant use of MTX or PRD were found between treatment groups.

Drug continuation rates

Drug continuation rates were analysed using Kaplan–Meier estimates (Figure 1). At 1 year, drug continuation rates for TCZ, IFX, ETN, and ADA were 89.4, 73.1, 85.9, and 78.2%, respectively, and at 2.5 years they were 79.3, 47.2, 77.7, and 54.5%, respectively. At 5 years, the drug continuation rates for TCZ, IFX, and ETN were 66.8, 29.8, and 61.9%, respectively. Of note, treatments with TCZ and ETN showed higher continuation rates than treatments with IFX or ADA (log-rank test, $p < 0.001$). The median (range) duration of treatment with TCZ, IFX, ETN, and ADA was 2.5 (0.1–12.6), 1.9 (0.0–7.7), 2.9 (0.0–11.3), and 1.3 (0.0–3.4) years, respectively. The duration of treatment with ADA was shorter

Table 1. Baseline characteristics of the patients.

	Tocilizumab (n = 97)	Infliximab (n = 103)	Etanercept (n = 143)	Adalimumab (n = 58)	p*
Age (years)	56.6 (27.2–81.8)	54.4 (21.5–80.3)	53.0 (18.7–77.5)	60.0 (18.0–76.7)	0.0267
Male:female	17:80	22:81	18:125	10:48	0.3297
Disease duration (years)	7.71 (0.57–38.3)	5.18 (0.23–32.9)	9.60 (0.18–39.4)	6.89 (0.35–30.8)	0.0114
DAS28-CRP(3)	4.38 (2.13–7.34) (n = 79)	4.20 (1.33–6.52) (n = 61)	4.19 (1.96–6.76) (n = 117)	3.84 (1.92–6.69) (n = 48)	0.0089
PRD use (%)	82.1	89.0	73.5	80.0	0.0321
PRD (mg/day)	6.0 (0.0–17.5) (n = 95)	7.5 (0.0–25.0) (n = 91)	5.0 (0.0–20.0) (n = 132)	5.0 (0.0–20.0) (n = 55)	< 0.0001
MTX use (%)	62.1	98.9	72.0	80.4	< 0.0001
MTX (mg/week)	6.0 (0.0–16.0) (n = 95)	8.0 (0.0–12.0) (n = 93)	6.0 (0.0–10.5) (n = 132)	6.0 (0.0–12.0) (n = 56)	< 0.0001
IP (%)	15.5	7.8	10.5	10.3	0.3832
Diabetes (%)	8.3	12.6	12.6	10.3	0.7390

DAS28-CRP(3), Disease Activity Score in 28 joints based on the C-reactive protein levels as assessed by three variables; PRD, prednisolone; MTX, methotrexate; IP, interstitial pneumonia.
Values are given as median (range) or percentage.
*By the χ^2 test for categorical variables and the Kruskal–Wallis test for continuous variables.

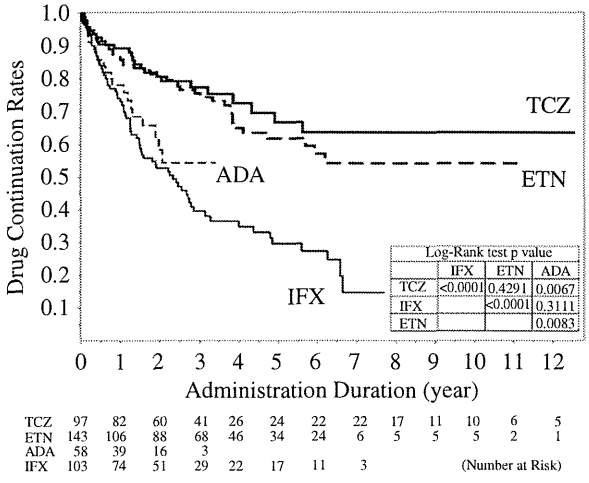

Figure 1. Kaplan–Meier curves for time to discontinuation of treatment with TCZ, IFX, ETN, and ADA. Cases discontinued due to remission or miscellaneous reasons were treated as censored cases. Drug continuation rates were compared using the log-rank test.

than that with the other biologics because ADA was not approved in Japan until June 2008.

Causes of discontinuation

The causes of discontinuation of the biologics are shown in Table 2. The difference between lack of efficacy and loss of efficacy was not clearly defined in this study. In fact, 88.9% (16/18) of discontinuation due to lack of efficacy occurred within 6 months and 98.4% (60/61) of discontinuation due to loss of efficacy occurred after over 6 months in our registry. The three anti-TNF drugs IFX, ETN, and ADA were mainly discontinued because of lack or loss of efficacy. By contrast, the most common cause of discontinuation of TCZ was any adverse event such as a serious infection. There were five deaths during the study period: one in the IFX group (due to IP), three in the TCZ group (bacterial arthritis, brain infarction, colon cancer), and one in the ETN group (suicide).

Cause-specific cumulative discontinuation rates were assessed using Kaplan–Meier estimates (Figure 2). The cumulative discontinuation rate due to lack or loss of efficacy rose linearly in each treatment group, and the gradients of the plots were large in the IFX and ADA groups, low in the TCZ group, and intermediate in the ETN group. Cumulative discontinuation rates due to adverse events increased linearly until approximately 2 years, after which the increase slowed down in each group. Of note, discontinuation due to hypersensitivity (including systemic or injection-site acute reaction) occurred mainly before 1.5 years in the IFX group. Cumulative discontinuation rates due to remission were low, up to 11% in each group.

Multivariate analyses

We calculated the HRs of discontinuation due to each specific cause using multivariate Cox proportional hazards regression (Table 3). [Adjustment was made for sex, age, disease duration, DAS28, concomitant dosage of PRD and MTX, and complications (IP and diabetes), unless stated otherwise.] Discontinuation due to overall unfavourable causes was significantly higher in the IFX and ADA groups than in the TCZ group [IFX vs. TCZ, HR 3.23, 95% confidence interval (CI) 1.81–5.94, $p < 0.0001$; ADA vs. TCZ, HR 2.82, 95% CI 1.42–5.58, $p = 0.0035$] and was not significantly different between TCZ and ETN (ETN vs. TCZ, HR 1.53, 95% CI 0.88–2.71, $p = 0.1304$). HRs for discontinuation due to lack or loss of efficacy were found to be significantly higher in the anti-TNF drug groups than in the TCZ group (IFX vs. TCZ,

AQ1 Table 2. Causes of treatment discontinuation.

Causes of discontinuation	Tocilizumab	Infliximab	Etanercept	Adalimumab
Lack of efficacy*	1 (3.7)	8 (10.3)	5 (8.8)	4 (16.0)
Loss of efficacy*	4 (14.8)	30 (38.5)	18 (31.6)	9 (36.0)
All adverse events	18 (66.7)	29 (37.2)	20 (35.1)	7 (28.0)
Hypersensitivity**	1 (3.7)	15 (19.2)	4 (7.0)	1 (4.0)
Serious infection	7 (25.9)	6 (7.7)	7 (12.3)	3 (12.0)
Malignancy	3 (11.1)	5 (6.4)	5 (8.8)	0
Vascular disease	2 (7.4)	0	1 (1.8)	0
Interstitial pneumonia	1 (3.7)	3 (3.8)	0	1 (4.0)
Skin rash	1 (3.7)	0	1 (1.8)	1 (4.0)
Neutropaenia	2 (7.4)	0	1 (1.8)	0
Other adverse events	1 appendicitis	0	1 suicide	1 elevation of CK
Miscellaneous**	2 (7.4)	4 (5.1)	7 (12.3)	2 (8.0)
Remission*	2 (7.4)	7 (9.0)	7 (12.3)	3 (12.0)
Total discontinuation	27	78	57	25

AQ2

Values are given as the number (percentage) of patients who discontinued biologics for each reason.
'Hypersensitivity' includes both systemic and injection-site reactions.
'Miscellaneous' include patient preferences, finances, and pregnancies.

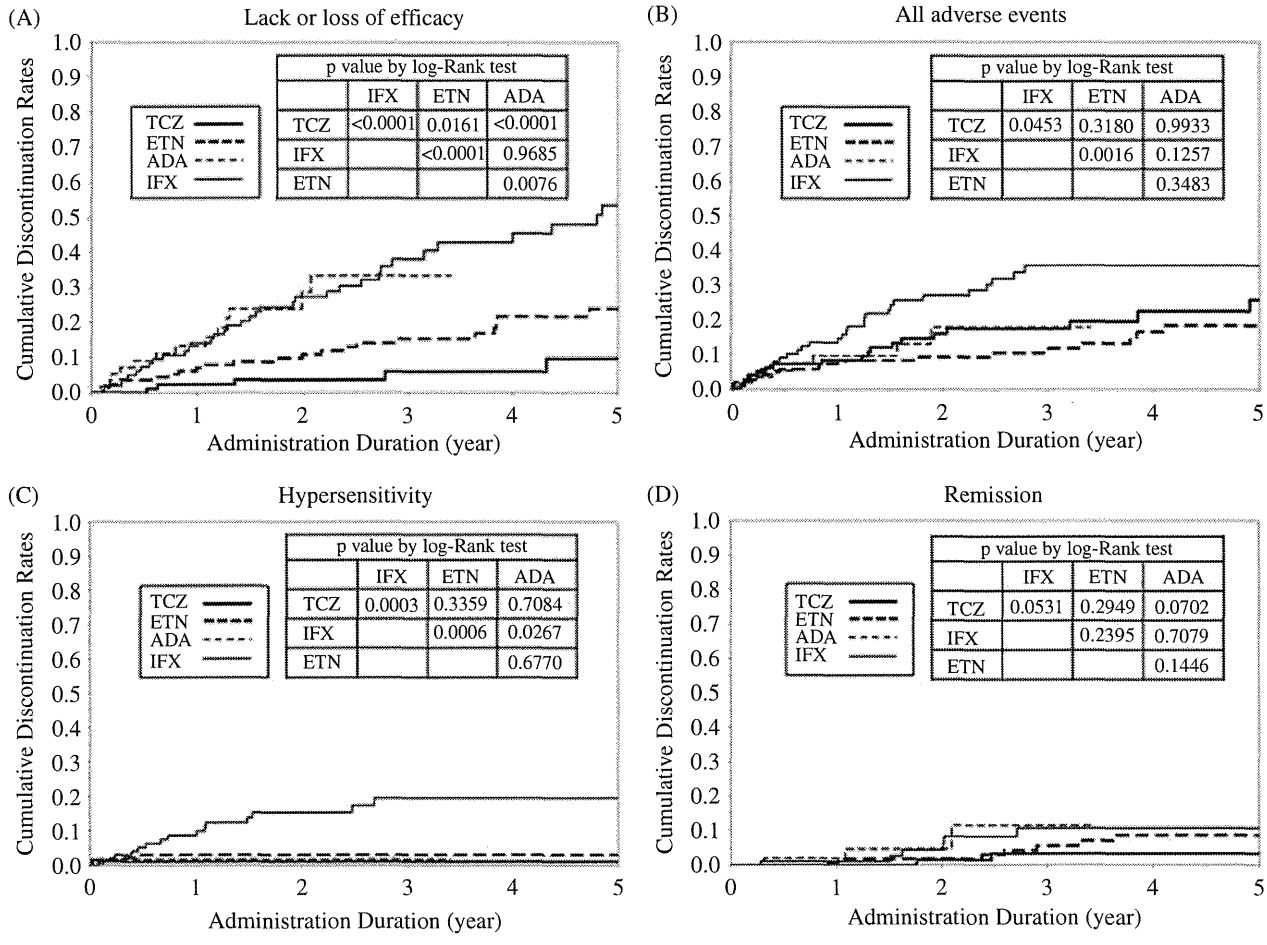

Figure 2. Cumulative discontinuation rates of the four drugs for specific reasons: (A) lack or loss of efficacy, (B) overall adverse events, (C) hypersensitivity (systemic or injection-site reaction), and (D) remission. Drug continuation rates were compared using the log-rank test.

HR 8.80, 95% CI 3.33–28.1, $p < 0.0001$; ETN vs. TCZ, HR 3.45, 95% CI 1.34–10.6, $p = 0.0088$; ADA vs. TCZ, HR 10.5, 95% CI 3.60–35.6, $p < 0.0001$).

HRs for discontinuation due to overall adverse events did not differ between treatment groups. HRs for discontinuation due to severe infection did not differ 210

Table 3. Hazard ratio (HRs) of discontinuation of the four drugs due to specific causes.

	Tocilizumab (reference)	Infliximab		Etanercept		Adalimumab		
		HR (95% CI)	p	HR (95% CI)	p	HR (95% CI)	p	
All unfavourable causes	1 (ref.)	3.23 (1.81–5.94)	< 0.0001	1.53 (0.88–2.71)	0.1304	2.82 (1.41–5.57)	0.0035	*1
Lack or loss of efficacy	1 (ref.)	8.80 (3.33–28.1)	< 0.0001	3.45 (1.34–10.6)	0.0088	10.5 (3.60–35.6)	< 0.0001	*1
All adverse events	1 (ref.)	1.61 (0.73–3.55)	0.2360	0.96 (0.47–1.96)	0.9084	0.93 (0.32–2.43)	0.8921	*1
Serious infection	1 (ref.)	0.96 (0.31–2.88)	0.9375	0.74 (0.25–2.16)	0.5696	0.83 (0.18–3.06)	0.7901	*2
Hypersensitivity	1 (ref.)	23.1 (2.73–548)	0.0022	1.79 (0.22–37.4)	0.6079	2.96 (0.11–83.3)	0.4735	*3
Remission	1 (ref.)	3.00 (0.63–21.8)	0.1734	1.34 (0.26–9.99)	0.7351	3.05 (0.47–24.4)	0.2337	*1

CI, confidence interval.
The results of Cox proportional hazards model analyses are shown.
*1 Adjusted for sex, age, disease duration, DAS28, concomitant dosages of PRD and MTX, and complications (IP or diabetes).
*2 Adjusted for age.
*3 Adjusted for age, disease duration, DAS28, and concomitant dosages of MTX and PRD.
'Hypersensitivity' includes both systemic and injection-site reactions.

significantly between treatment groups after adjustment for age. HRs for discontinuation due to hypersensitivity (systemic or injection site) were significantly higher in the IFX group than in the other groups (IFX vs. TCZ, HR 23.1, 95% CI 2.73–548, p = 0.0022), after adjustment for sex, age, DAS28, disease duration, and concomitant dosage of MTX or PRD. However, HRs for discontinuation due to remission did not differ significantly between treatment groups.

Discussion

To the best of our knowledge, this is the first report to compare retention (> 3 years) of initial biologics, including TCZ, in biologic-naïve patients with RA. In this study, TCZ and ETN showed similar retention for the treatment of RA, and both were better than IFX and ADA. Multivariate analyses showed that this difference was not mainly attributable to adverse events, such as infections, but to durability of efficacy.

In general, our results are consistent with four previous observational studies reporting continuation rates for anti-TNF drugs (10–14). From the Lombardy Rheumatology Network (LOHREN) registry (n = 1064), Marchesoni et al showed that treatment continuation rates for IFX, ETN, and ADA were approximately 56, 57, and 72%, respectively, at 2.5 years. The risk of discontinuation was similar for poor efficacy and adverse events (10). In the Swiss Clinical Quality Management RA cohort (n = 2364), Du Pan et al showed that treatment continuation rates for IFX, ETN, and ADA were approximately 51, 58, and 61%, respectively, at 2.5 years (11). Lack or loss of drug efficacy represented the most common single cause of treatment discontinuation. In an analysis of the DANBIO registry (n = 2326), which is a nationwide Danish registry of rheumatology patients, Hetland et al showed that continuation rates for IFX, ETN, and ADA were approximately 44, 67, and 60%, respectively, at 2.5 years. Discontinuation due to lack of efficacy was more common than discontinuation due to adverse events (12). Analysing the Italian Study Group on Early Arthritides (GISEA) registry (n = 853), Iannone et al found that continuation rates for IFX, ETN, and ADA were approximately 52, 65, and 52%, respectively, at 2.5 years (13). These four reports agreed that IFX showed the lowest continuation rate among the three anti-TNF drugs and that lack or loss of efficacy was the main cause of discontinuation. These findings are consistent with the results from our registry.

The 1-year drug continuation rate of TCZ in real-life clinical practice was analysed in two studies (6, 7). Takeuchi et al reported a continuation rate of 71.1% for TCZ at 52 weeks in the REACTION cohort study (n = 232) (6). Similarly, Leffers et al reported a continuation rate of 64% for TCZ at 48 weeks in the DANBIO registry (n = 178) (7). The continuation rate of TCZ was reported as 88, 75, and 68% at 1, 2.5, and 5 years, respectively, in a combined analysis of six clinical studies and their extensions in Japan (n = 601) conducted by Nishimoto et al (14). The continuation rate of TCZ reported by Nishimoto et al was similar to that in our registry, which was higher than that reported in the REACTION study and DANBIO registry. This difference may be due to the fact that the former two studies included patients who participated in clinical studies whereas the latter included non-biologic-naïve patients. Of note, all these studies, including ours, found a similar tendency, indicating that TCZ is discontinued more commonly due to adverse events than to lack or loss of efficacy.

Comparisons of TCZ and anti-TNF drugs in Japanese patients with RA have been made using data from the CABUKI registry (8) and the REAL registry (9). From the CABUKI registry (n = 247, including non-biologic-naïve patients), Yoshida et al concluded that TCZ and anti-TNF drugs showed similar drug retention rates (8). However, the CABUKI registry was considered to be too small to identify drug continuation rates longer than 1 year because only seven patients were still taking TCZ at

1.5 years. From the REAL registry (n = 1022, including non-biologic-naïve patients), Sakai et al compared TCZ and anti-TNF drugs in Japanese patients with RA and showed that the continuation rates of TCZ, IFX, and ETN at 2.5 years were approximately 67, 67, and 72%, respectively, and concluded that IFX and TCZ were significantly associated with treatment discontinuation due to adverse events compared with ETN (9). The conclusion from the REAL registry differs from our results. This disparity may be explained by two differences between the studies. First, the observation period of the REAL registry was shorter than that of our registry. Second, the continuation rates of anti-TNF drugs in the REAL study were much higher than in our study and in previous reports. These differences suggest that unreported factors, such as the dosage of IFX or changes in the concomitant dosage of DMARDs and PRD, raised the continuation rates of anti-TNF drugs in that study. The continuation rate of TCZ in the REAL study was slightly lower than that in our registry and in the report of Nishimoto et al (14), probably because Nishimoto et al reported their results on the basis of clinical studies and our registry also included 29 patients (29.9%) who participated in clinical trials.

Our study has several limitations. First, our study was observational; therefore, some biases may be present, such as in the selection of patients and the choice of the biologics, although similar biases are common to all observational studies. Indeed, ADA was administered to patients who were older than those administered ETN and IFX. This bias may have lowered the observed retention rate of ADA. Concomitant use of methotrexate (MTX) was significantly higher in patients who were administered IFX than other biologics. This bias may have elevated the retention rate of IFX. Furthermore, TCZ was administered to patients who had significantly higher DAS28 scores than those administered ADA. ETN was administered to patients who had longer disease duration than those administered IFX. Concomitant glucocorticoid dosage was the highest in the IFX group, the lowest in the ETN and ADA groups, and intermediate in the TCZ group. However, the influence of these biases was unclear. Nonetheless, shorter disease duration was associated with discontinuation due to both poor efficacy and remission in our study (data not shown). Given the relatively small sample size in this study (401 patients), we limited the number of variables in the multivariate analyses and the reported 95% CIs were broadened. Nevertheless, observational cohort studies such as this one offer the only way to assess retention of biologics in real clinical settings. Importantly, TCZ clearly showed better retention than IFX and ADA, even in our small cohort. However, changes in the dosage of IFX or concomitant DMARDs and PRD were not analysed in this study, and further study is necessary to determine risk factors for discontinuation, particularly due to infection. For example, the dosage of PRD at baseline was not detected as a risk factor for discontinuation due to infections in our study (data not shown).

In conclusion, our cohort study showed that TCZ had excellent retention in the treatment of RA, and the continuation rate of TCZ was higher than that of IFX and ADA. The continuation rate of ETN was not statistically different from that of TCZ. Discontinuation due to lack or loss of efficacy was significantly less common in the TCZ-treated group. Although TCZ was discontinued mainly due to adverse events, discontinuation due to adverse events was not significantly different between TCZ and anti-TNF drugs.

Acknowledgements

We thank the following rheumatologists for their critical comments and suggestions and for responding to our inquiries: N Nishimoto, S Ohshima, J Hashimato, R Yasunami, H Ohwaki, K Takahi, K Saito, K Yamamoto, W Ito, M Kai, Y Ito, S Sakito, O Akahori, T Takashima, A Nampei, T Ikawa, S Hirohata, Y Kita, S Fujii, T Harada, H Ninomiya, M Yajima, and M Takei.

This work was supported by research grants from the Ministry of Education, Culture, Sports, Science, and Technology of Japan (A.K.); grants-in-aid from the Ministry of Health, Labour and Welfare (A.K.); Funding Programme for Next-Generation World-Leading Researchers (NEXT Program) (A.K.); and Special Coordination Funds for Promoting Science and Technology (A.K.).

References

1. Singh JA, Furst DE, Bharat A, Curtis JR, Kavanaugh AF, Kremer JM, et al. 2012 Update of the 2008 American College of Rheumatology recommendations for the use of disease-modifying antirheumatic drugs and biologic agents in the treatment of rheumatoid arthritis. Arthritis Care Res 2012;64:625–39.
2. Furst DE, Keystone EC, Braun J, Breedveld FC, Burmester GR, De Benedetti F, et al. Updated consensus statement on biological agents for the treatment of rheumatic diseases, 2011. Ann Rheum Dis 2012;71:2–45.
3. Kristensen LE, Jakobsen AK, Bartels EM, Geborek P, Bliddal H, Saxne T, et al. The number needed to treat for second-generation biologics when treating established rheumatoid arthritis: a systematic quantitative review of randomized controlled trials. Scand J Rheumatol 2011;40:1–7.
4. Takeuchi T, Kameda H. The Japanese experience with biologic therapies for rheumatoid arthritis. Nat Rev Rheumatol 2010;6:644–52.
5. Nishimoto N, Ito K, Takagi N. Safety and efficacy profiles of tocilizumab monotherapy in Japanese patients with rheumatoid arthritis: meta-analysis of six initial trials and five long-term extensions. Mod Rheumatol 2010;20:222–32.
6. Takeuchi T, Tanaka Y, Amano K, Hoshi D, Nawata M, Nagasawa H, et al. Clinical, radiographic and functional effectiveness of tocilizumab for rheumatoid arthritis patients – REACTION 52-week study. Rheumatology (Oxford) 2011;50:1908–15.
7. Leffers HC, Ostergaard M, Glintborg B, Krogh NS, Foged H, Tarp U, et al. Efficacy of abatacept and tocilizumab in patients with rheumatoid arthritis treated in clinical practice: results from the nationwide Danish DANBIO registry. Ann Rheum Dis 2011;70:1216–22.
8. Yoshida K, Tokuda Y, Oshikawa H, Utsunomiya M, Kobayashi T, Kimura M, et al. An observational study of tocilizumab and TNF-alpha inhibitor use in a Japanese community hospital: different remission rates, similar drug survival and safety. Rheumatology (Oxford) 2011;50:2093–9.

9. Sakai R, Tanaka M, Nanki T, Watanabe K, Yamazaki H, Koike R, et al. Drug retention rates and relevant risk factors for drug discontinuation due to adverse events in rheumatoid arthritis patients receiving anticytokine therapy with different target molecules. Ann Rheum Dis 2012;71:1820–6.
10. Marchesoni A, Zaccara E, Gorla R, Bazzani C, Sarzi-Puttini P, Atzeni F, et al. TNF-alpha antagonist survival rate in a cohort of rheumatoid arthritis patients observed under conditions of standard clinical practice. Ann N Y Acad Sci 2009;1173:837–46.
11. Du Pan SM, Dehler S, Ciurea A, Ziswiler HR, Gabay C, Finckh A, et al. Comparison of drug retention rates and causes of drug discontinuation between anti-tumor necrosis factor agents in rheumatoid arthritis. Arthritis Rheum 2009;61:560–8.
12. Hetland ML, Christensen IJ, Tarp U, Dreyer L, Hansen A, Hansen IT, et al. Direct comparison of treatment responses, remission rates, and drug adherence in patients with rheumatoid arthritis treated with adalimumab, etanercept, or infliximab: results from eight years of surveillance of clinical practice in the nationwide Danish DANBIO registry. Arthritis Rheum 2010;62:22–32.
13. Iannone F, Gremese E, Atzeni F, Biasi D, Botsios C, Cipriani P, et al. Longterm retention of tumor necrosis factor-α inhibitor therapy in a large Italian cohort of patients with rheumatoid arthritis from the GISEA Registry: an appraisal of predictors. J Rheumatol 2012;39:1179–84.
14. Tanaka T, Kishimoto T. Immunotherapeutic implication of IL-6 blockade. Immunotherapy 2012;4:87–105.
15. Bykerk VP, Ostör AJ, Alvaro-Gracia J, Pavelka K, Ivorra JA, Graninger W, et al. Tocilizumab in patients with active rheumatoid arthritis and inadequate responses to DMARDs and/or TNF inhibitors: a large, open-label study close to clinical practice. Ann Rheum Dis 2012;71:1950–4.
16. Emery P, Keystone E, Tony HP, Cantagrel A, van Vollenhoven R, Sanchez A, et al. IL-6 receptor inhibition with tocilizumab improves treatment outcomes in patients with rheumatoid arthritis refractory to anti-tumour necrosis factor biologicals: results from a 24-week multicentre randomised placebo-controlled trial. Ann Rheum Dis 2008;67:1516–23.
17. Nishimoto N, Hashimoto J, Miyasaka N, Yamamoto K, Kawai S, Takeuchi T, et al. Study of active controlled monotherapy used for rheumatoid arthritis, an IL-6 inhibitor (SAMURAI): evidence of clinical and radiographic benefit from an x ray reader-blinded randomised controlled trial of tocilizumab. Ann Rheum Dis 2007;66:1162–7.
18. Nishimoto N, Miyasaka N, Yamamoto K, Kawai S, Takeuchi T, Azuma J. Long-term safety and efficacy of tocilizumab, an anti-IL-6 receptor monoclonal antibody, in monotherapy, in patients with rheumatoid arthritis (the STREAM study): evidence of safety and efficacy in a 5-year extension study. Ann Rheum Dis 2009;68:1580–4.
19. Nishimoto N, Yoshizaki K, Miyasaka N, Yamamoto K, Kawai S, Takeuchi T, et al. Treatment of rheumatoid arthritis with humanized anti-interleukin-6 receptor antibody – a multicenter, double-blind, placebo-controlled trial. Arthritis Rheum 2004;50:1761–9.
20. Smolen JS, Beaulieu A, Rubbert-Roth A, Ramos-Remus C, Rovensky J, Alecock E, et al. Effect of interleukin-6 receptor inhibition with tocilizumab in patients with rheumatoid arthritis (OPTION study): a double-blind, placebo-controlled, randomised trial. Lancet 2008;371:987–97.
21. Genovese MC, McKay JD, Nasonov EL, Mysler EF, da Silva NA, Alecock E, et al. Interleukin-6 receptor inhibition with tocilizumab reduces disease activity in rheumatoid arthritis with inadequate response to disease-modifying antirheumatic drugs: the tocilizumab in combination with traditional disease-modifying antirheumatic drug therapy study. Arthritis Rheum 2008;58:2968–80.
22. Maini RN, Taylor PC, Szechinski J, Pavelka K, Broell J, Balint G, et al. Double-blind randomized controlled clinical trial of the interleukin-6 receptor antagonist, tocilizumab, in European patients with rheumatoid arthritis who had an incomplete response to methotrexate. Arthritis Rheum 2006;54:2817–29.
23. Arnett FC, Edworthy SM, Bloch DA, McShane DJ, Fries JF, Cooper NS, et al. The American Rheumatism Association 1987 revised criteria for the classification of rheumatoid arthritis. Arthritis Rheum 1988;31:315–24.
24. Aletaha D, Neogi T, Silman AJ, Funovits J, Felson DT, Bingham CO, et al. 2010 Rheumatoid arthritis classification criteria: an American College of Rheumatology/European League Against Rheumatism collaborative initiative. Arthritis Rheum 2010;62:2569–81.
25. Koike R, Harigai M, Atsumi T, Amano K, Kawai S, Saito K, et al. Japan College of Rheumatology 2009 guidelines for the use of tocilizumab, a humanized anti-interleukin-6 receptor monoclonal antibody, in rheumatoid arthritis. Mod Rheumatol 2009;19:351–7.
26. Koike R, Takeuchi T, Eguchi K, Miyasaka N; Japan College of Rheumatology. Update on the Japanese guidelines for the use of infliximab and etanercept in rheumatoid arthritis. Mod Rheumatol 2007;17:451–8.
27. Prevoo ML, van 't Hof MA, Kuper HH, van Leeuwen MA, van de Putte LBA, van Riel P. Modified disease activity scores that include twenty-eight-joint counts. Development and validation in a prospective longitudinal study of patients with rheumatoid arthritis. Arthritis Rheum 1995;38:44–8.
28. von Elm E, Altman DG, Egger M, Pocock SJ, Gotzsche PC, Vandenbroucke JP, et al. The Strengthening the Reporting of Observational Studies in Epidemiology (STROBE) statement: guidelines for reporting observational studies. Prev Med 2007;45:247–51.

nature COMMUNICATIONS

ARTICLE

Received 8 Jun 2012 | Accepted 20 Dec 2012 | Published 29 Jan 2013

DOI: 10.1038/ncomms2420 OPEN

A point mutation in *Semaphorin 4A* associates with defective endosomal sorting and causes retinal degeneration

Satoshi Nojima[1,2], Toshihiko Toyofuku[1], Hiroyuki Kamao[3,4], Chie Ishigami[3], Jun Kaneko[3], Tatsusada Okuno[1,5], Hyota Takamatsu[1], Daisuke Ito[1,6], Sujin Kang[1,6], Tetsuya Kimura[1,6], Yuji Yoshida[1,6], Keiko Morimoto[1,6], Yohei Maeda[1,7], Atsushi Ogata[1,6], Masahito Ikawa[8], Eiichi Morii[2], Katsuyuki Aozasa[2], Junichi Takagi[9], Masayo Takahashi[3] & Atsushi Kumanogoh[1,6,10]

Semaphorin 4A (Sema4A) has an essential role in photoreceptor survival. In humans, mutations in *Sema4A* are thought to contribute to retinal degenerative diseases. Here we generate a series of knock-in mouse lines with corresponding mutations (D345H, F350C or R713Q) in the *Sema4A* gene and find that Sema4A^{F350C} causes retinal degeneration phenotypes. The F350C mutation results in abnormal localization of the Sema4A protein, leading to impaired endosomal sorting of molecules indispensable for photoreceptor survival. Additionally, protein structural modelling reveals that the side chain of the 350th amino acid is critical to retain the proper protein conformation. Furthermore, *Sema4A* gene transfer successfully prevents photoreceptor degeneration in *Sema4A*$^{F350C/F350C}$ and *Sema4A*$^{-/-}$ mice. Thus, our findings not only indicate the importance of the Sema4A protein conformation in human and mouse retina homeostasis but also identify a novel therapeutic target for retinal degenerative diseases.

[1] Department of Immunopathology, WPI Immunology Frontier Research Center, Osaka University, Suita City, Osaka 565-0871, Japan. [2] Department of Pathology, Osaka University Graduate School of Medicine, Osaka University, Suita City, Osaka 565-0871, Japan. [3] Laboratory for Retinal Regeneration, RIKEN Center for Developmental Biology, Kobe 650-0047, Japan. [4] Department of Ophthalmology, Postgraduate School of Kawasaki Medical School, Kawasaki Medical School, Kurashiki City, Okayama 701-0192, Japan. [5] Department of Neurology, Graduate School of Medicine, Osaka University, Suita City, Osaka 565-0871, Japan. [6] Department of Respiratory Medicine, Allergy and Rheumatic Disease, Graduate School of Medicine, Osaka University, Suita City, Osaka 565-0871, Japan. [7] Department of Otorhinolaryngology-Head and Neck Surgery, Graduate School of Medicine, Osaka University, Suita City, Osaka 565-0871, Japan. [8] Animal Resource Center for Infectious Diseases, Research Institute for Microbial Diseases, Osaka University, Suita, Osaka 565-0871, Japan. [9] Laboratory of Protein Synthesis and Expression, Institute for Protein Research, Osaka University, Suita City, Osaka 565-0871, Japan. [10] JST, CREST, Suita City, Osaka 565-0871, Japan. Correspondence and requests for materials should be addressed to T.T. (email: toyofuku@imed3.med.osaka-u.ac.jp) or to A.K. (email: kumanogo@imed3.med.osaka-u.ac.jp).

The major cause of adult blindness in industrialized countries is the progressive dysfunction and death of retinal photoreceptors. Retinal photoreceptor degeneration is one of the most genetically heterogeneous disorders in humans. Inherited forms of retinal photoreceptor degeneration are defined by their predominantly monogenic inheritance and are a common cause of visual impairment, with a prevalence of ~1 in 3,000 (refs 1, 2). Although many genes have been linked to a photoreceptor degenerative disease phenotype, the mechanisms by which most of these genes lead to this disorder are not fully understood.

Semaphorins were initially identified as axonal guidance cues that determine the direction and migration of neurons during neurogenesis[3]. In addition, accumulating evidence has shown that semaphorins have diverse functions in other physiological and pathogenic processes, including vascular development[4], tumour progression[5], heart development[6] and immune responses[7,8]. Semaphorin 4A (Sema4A) is a class IV transmembrane-type semaphorin. Previously, Rice *et al.*[9] reported that inserting a gene-trap vector into intron 11 of the mouse *Sema4A* gene resulted in the loss of retinal photoreceptors. Consistent with their findings, we recently determined that Sema4A-deficient (*Sema4A*$^{-/-}$) mice display severe photoreceptor degeneration[10]. Notably, we demonstrated that Sema4A, which is expressed in retinal pigment epithelial (RPE) cells, regulates distinct endosomal sorting pathways that are critical for photoreceptor survival and phototransduction during the transition between daylight and darkness[10]. Thus, *Sema4A* is thought to be one of the genes responsible for retinal degenerative diseases. In fact, three mutations, D345H (345GAC→CAC; D→H), F350C (350TTT→TGT; F→C) and R713Q (713CGG→CAG; R→Q), in the human *Sema4A* gene have been reported in patients with retinal degenerative diseases based on sequencing of the *Sema4A* gene from 190 unrelated patients suffering from a variety of retinal degenerative diseases, including retinitis pigmentosa and cone rod dystrophy[11]. However, it has not been determined whether these mutations are really responsible for retinal degeneration, and if so, how mutations in the *Sema4A* gene induce pathogenesis.

In this report, we generated a series of knock-in mouse lines with mutations (D345H, F350C and R713Q) in the *Sema4A* gene in order to examine the impact of these mutations on the pathogenesis of retinal degenerative diseases. We found that a single point mutation, F350C, caused severe degeneration in photoreceptor cells. In addition, we determined that the pathogenicity of the F350C mutation is due to severe structural defects and resultant mis-localization of the Sema4A protein in RPE cells, which led to impaired endosomal sorting. Furthermore, we provided evidence that *Sema4A* is a therapeutic target for retinal degenerative diseases using virus-mediated gene therapy.

Results

***Sema4A*$^{F350C/F350C}$ mice exhibit retinal degeneration.** We first generated a series of knock-in mouse lines that express wild-type (WT) or mutated Sema4A proteins. As the amino-acid sequence of Sema4A is highly conserved between humans and mice, with the 345th, 350th and 713th amino acids being identical, we constructed four knock-in vectors to generate mice with these respective mutations (Fig. 1a). Full-size cDNA fragments of WT *Sema4A* or mutated *Sema4A* (D345H, F350C or R713Q) fused to enhanced green fluorescent protein (EGFP) at the carboxy terminus were inserted into exon 2 and exon 3 of the *Sema4A* gene. This series of homozygous knock-in mice appeared normal at birth, developed normally and were fertile, as it is the case for *Sema4A*$^{-/-}$ mice. Every mutant protein was expressed in tissues (Fig. 1b).

Photoreceptor homeostasis is functionally and mechanically supported by RPE cells, which closely interact with photoreceptors via microvilli that interdigitate with the adjacent photoreceptor outer segment. RPE cells perform specialized functions for photoreceptors, including supplying nutrients and factors that protect against light-induced oxidative damage[12]. Immunohistochemistry with an anti-green fluorescent protein (GFP) antibody showed that Sema4A localized at the apical surface of the plasma membrane in RPE cells (Fig. 1c), which is consistent with our previous studies[10]. We then examined the histopathology of the respective *Sema4A* knock-in mice. Of note, only *Sema4A*$^{F350C/F350C}$ mice exhibited changes in retinal photoreceptors that were compatible with *Sema4A*$^{-/-}$ mice (Fig. 2a). The outer segment of photoreceptors in *Sema4A*$^{F350C/F350C}$ retina was severely disrupted at 2 weeks of age, followed by a complete loss of photoreceptors at 4 weeks of age (Supplementary Fig. S1). Electroretinography (ERG) monitoring confirmed these histological findings (Fig. 2b). A TdT-mediated dUTP nick end labelling (TUNEL) assay demonstrated that *Sema4A*$^{F350C/F350C}$ retina exhibited a marked increase in the number of apoptotic cells in the outer nuclear layer under illumination (Fig. 2c,d), which was similar to that observed in *Sema4A*$^{-/-}$ mice[10]. By contrast, *Sema4A*$^{D345H/D345H}$ and *Sema4A*$^{R713Q/R713Q}$ mice did not exhibit retinal degeneration (Fig. 2a). In addition, *Sema4A*$^{D345H/+}$, *Sema4A*$^{F350C/+}$ and *Sema4A*$^{R713Q/+}$ mice did not show any retinal defects (Supplementary Fig. S2). Although compound D345H/F350C heterozygous mutations were reported to be associated with retinal degenerative diseases in humans[11], knock-in mice carrying these mutations did not exhibit this phenotype (Fig. 2a). These findings indicate the importance of the 350th amino acid in the function of Sema4A protein.

The Sema4A^{F350C} protein is mis-localized in RPE cells. These findings raise the question of why the F350C mutation results in impaired Sema4A functions, even though the expression of this mutant protein is not severely impaired in tissues (Fig. 1b). To elucidate this question, we examined protein localization in the retina using the same series of mutant *Sema4A* knock-in mice. Interestingly, immunohistochemistry revealed that the Sema4A^{F350C}-EGFP protein was abnormally localized. Sema4A^{F350C}-EGFP remained in the cytosol, while Sema4A^{WT}-EGFP, Sema4A^{D345H}-EGFP and Sema4A^{R713Q}-EGFP localized to the surface of RPE cells in the retinas of mutant knock-in mice (Fig. 3a) and to the surface of primary cultured RPE cells derived from mutant knock-in mice (Fig. 3b). To confirm these findings, we prepared constructs expressing Sema4A^{WT}-EGFP, Sema4A^{D345H}-EGFP, Sema4A^{F350C}-EGFP and Sema4A^{R713Q}-EGFP for *in vitro* assays, and examined their cellular localization by introducing them into COS-7 cells or a human RPE-derived cell line, ARPE-19 cells. As expected, the Sema4A^{F350C}-EGFP protein failed to reach the plasma membrane, while Sema4A^{WT}-EGFP, Sema4A^{D345H}-EGFP and Sema4A^{R713Q}-EGFP localized to the plasma membrane (Fig. 3c,d). These results indicate that photoreceptor degeneration in *Sema4A*$^{F350C/F350C}$ mice was due to defects in Sema4A protein localization and distribution in RPE cells.

In addition, the Sema4A^{F350C} protein did not impair the cell surface expression of the Sema4A^{WT} protein (Fig. 4a,b), indicating that the F350C mutation does not function in a dominant-negative manner.

The Sema4A^{F350C} protein results in impaired endosomal sorting. Moreover, Blue-native PAGE (BN-PAGE) analysis, which separates proteins under native conditions[13], indicated that the structural integrity of Sema4A was compromised by F350C

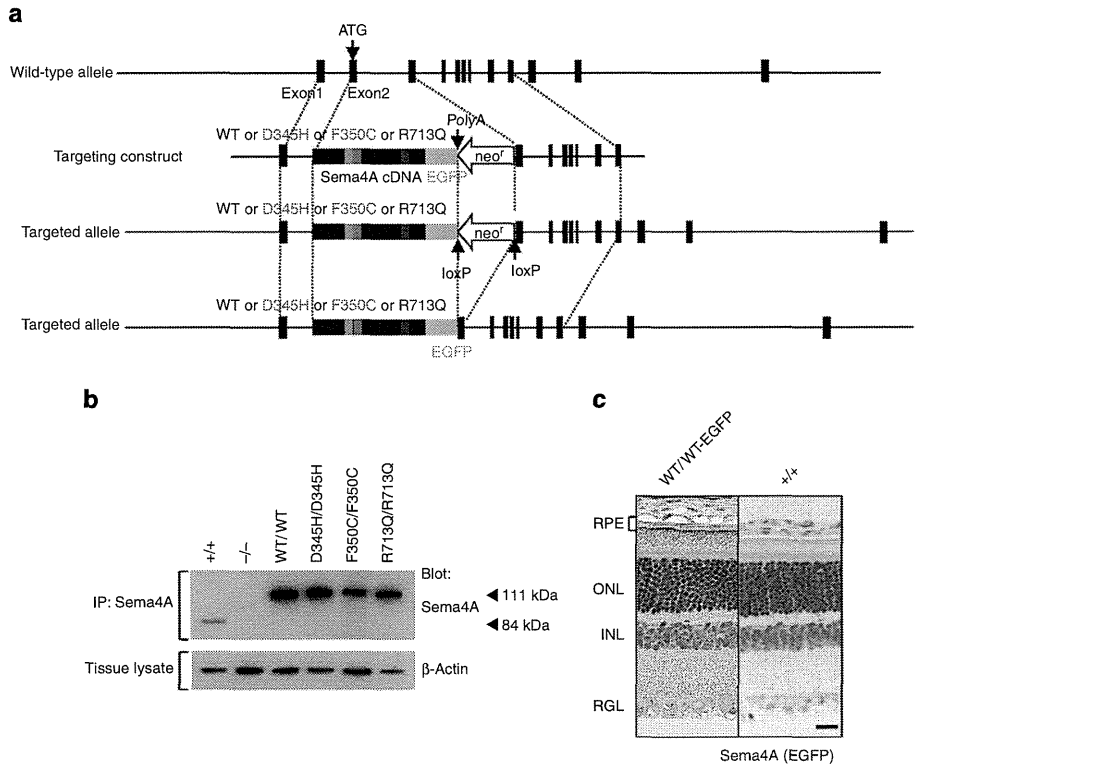

Figure 1 | Generation of knock-in mice. (**a**) Schematic diagram of the endogenous mouse locus for the *Sema4A* knock-in vectors and the resulting Sema4A proteins after homologous recombination. Full-length cDNA fragments of WT *Sema4A* or mutated *Sema4A* (D345H, F350C or R713Q) fused with EGFP at the C-terminus were inserted into exon 2 and exon 3 of the *Sema4A* gene. The neomycin resistance gene was flanked by loxP sites so that it could be excised upon expression of Cre recombinase. The gene structure of the WT *Sema4A* allele (top), *Sema4A*-targeting construct (second row) and the resulting *Sema4A*-targeted allele in which the neomycin resistance gene was (bottom) or was not (third row) excised. (**b**) Expression of Sema4A proteins in the brain tissues of knock-in mice. Brain tissues from WT (*Sema4A*$^{+/+}$), *Sema4A*$^{WT/WT}$, *Sema4A*$^{D345H/D345H}$, *Sema4A*$^{F350C/F350C}$, *Sema4A*$^{R713Q/R713Q}$ and *Sema4A*$^{-/-}$ (negative control) mice were lysed and subjected to immunoprecipitation (IP) and Western blot analyses using an anti-Sema4A antibody. The 111-kDa bands represent the mutant Sema4A-EGFP proteins (EGFP-tagged), while the 84-kDa band represents the endogenous wild-type Sema4A protein. All series of knock-in mice expressed sufficient amounts of Sema4A protein. (**c**) Paraffin sections of *Sema4A*$^{WT/WT}$ or wild-type (*Sema4A*$^{+/+}$) (negative control) retinas were examined by immunohistochemistry with an anti-GFP antibody. Sema4A normally localizes at the apical surface of RPE cells in the retina. Scale bar, 50 μm.

mutation; the Sema4A^{F350C} protein behaved as high-molecular-weight aggregates on the gel, whereas the other Sema4A proteins migrated as distinct bands corresponding to the monomer and dimer (Fig. 5a). In order to explore more about the critical roles of F350 in the Sema4A structure, we prepared a series of Sema4A expression constructs that harbour various mutations in this position, including methionine, tyrosine, glycine and serine (F350M, F350Y, F350G and F350S, respectively). We introduced these expression constructs into ARPE-19 cells or COS-7 cells and examined whether the respective proteins could reach the cell surface. Interestingly, F350M and F350Y, but not F350G and F350S, could reach the plasma membrane (Fig. 5b,c). The result indicates that the mutation is tolerated when F350 is substituted with relatively large amino acids (that is, Met and Tyr), while replacement with small residues (that is, Cys, Gly, and Ser) is detrimental.

Recently, the determination of the crystal structures of semaphorin ectodomains, particularly in complex with their cognate plexin receptors, has led to remarkable progress in our understanding of the structural basis for semaphorin function[14–18]. To investigate the structural background of the differential effect of each mutation on the function, we built a structural model of mouse Sema4A ectodomain using the structure of human Sema4D fragment as a template (PDB ID: 1OLZ)[15]. In the model, F350 is located far from the predicted plexin-binding surface (Fig. 5d), suggesting that the functional defect exhibited by the mutants is not attributable to a specific loss of plexin-binding activity. Closer inspection of the model revealed that the residue is only partially exposed on the protein surface (Fig. 5d), with its large aromatic side chain nestled in a pocket created by many hydrophobic residues (Fig. 5e). Therefore, mutation of this residue to amino acids with smaller side chain would create significant vacant space in the protein interior, which is known to harm the overall stability of the protein[19]. Thus, our study clearly demonstrated the importance of the correct cellular localization of Sema4A in RPE cells, which can be fundamentally disturbed by the lack of only a few atoms in a critical amino-acid residue.

We previously demonstrated that Sema4A exerts a unique function in the retina, namely by regulating the endosomal sorting of molecules that are indispensable for the phototransduction and survival of photoreceptors[10]. Sema4A regulates two distinct endosomal sorting pathways. First, Sema4A sorts prosaposin, an important antiapoptotic factor, to the plasma membrane of RPE cells, where it is subsequently secreted via exosomes. Second, Sema4A sorts retinoid-binding proteins, including cellular retinaldehyde-binding protein (CRALBP),

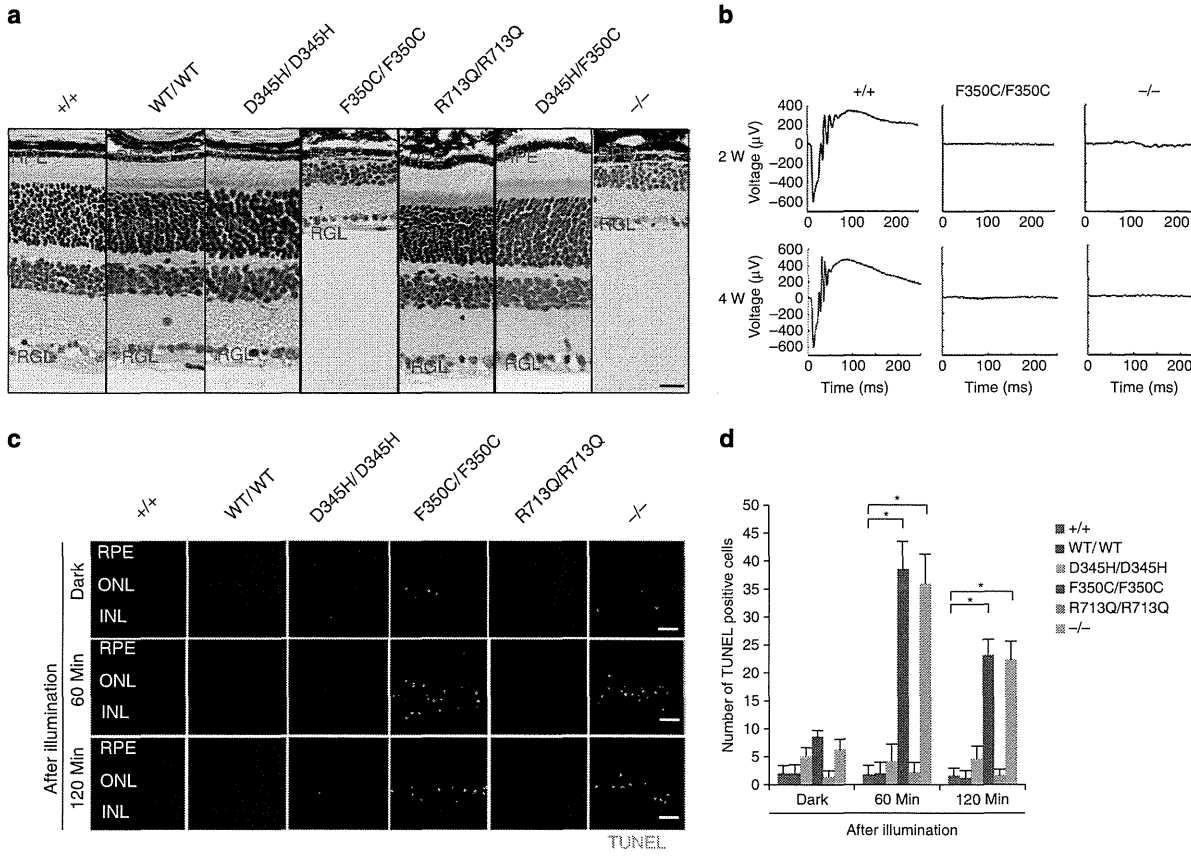

Figure 2 | Light-induced photoreceptor damage in retinas of *Sema4A*$^{F350C/F350C}$ mice. (**a**) Hematoxylin and eosin (HE) staining of retinas in 4-week-old wild-type (Sema4A$^{+/+}$), *Sema4A*$^{WT/WT}$, *Sema4A*$^{D345H/D345H}$, *Sema4A*$^{F350C/F350C}$, *Sema4A*$^{R713Q/R713Q}$, *Sema4A*$^{D345H/F350C}$ and Sema4A-deficient (*Sema4A*$^{-/-}$) mice. Among them, *Sema4A*$^{F350C/F350C}$ and *Sema4A*$^{-/-}$ retinas showed loss of the outer nuclear layer. Scale bar, 50 μm. RPE, retinal pigment epithelium; ONL, outer nuclear layer; INL, inner nuclear layer; RGL, retinal ganglion layer. (**b**) ERG responses to single flashes were recorded using wild-type (*Sema4A*$^{+/+}$), *Sema4A*$^{F350C/F350C}$ and *Sema4A*$^{-/-}$ mice in a scotopic condition at 2 or 4 weeks of age. Virtually no ERG responses were detected in *Sema4A*$^{-/-}$ and *Sema4A*$^{F350C/F350C}$ retinas as early as 2 weeks of age. (**c**) Representative images from the TUNEL assay using P10 mouse retinas after 0, 60 and 120 min of light exposure. Scale bar, 50 μm. (**d**) Histogram showing the average number of TUNEL-positive cells (± s.e.m.; $n = 5$–10) in retinas. *$P < 0.01$ (Student's *t*-test). Photoreceptor apoptosis peaked in *Sema4A*$^{-/-}$ and *Sema4A*$^{F350C/F350C}$ retinas after 60 min of exposure. Data are representative of three independent experiments.

which is involved in the transport of retinoids to photoreceptors during dark adaptation and the retinoid cycle, to the surface of RPE cells. Indeed, similar to *Sema4A*$^{-/-}$ cells, RPE cells from *Sema4A*$^{F350C/F350C}$ retinas expressed lower levels of prosaposin in secreted H_2O_2-induced exosomes (Fig. 5f,g), indicating that endosomal sorting is impaired in *Sema4A*$^{F350C/F350C}$ RPE cells as well as *Sema4A*$^{-/-}$ RPE cells. CRALBP also failed to distribute to the surface of RPE cells (Fig. 5h,i). These results indicate that the endosomal sorting function of Sema4A was severely impaired by the F350C mutation.

***Sema4A* gene transfer prevents retinal degeneration.** For potential gene therapy, we finally performed lentivirus-mediated *Sema4A* gene transfer experiments to determine whether this method could prevent retinal photoreceptor degeneration. According to a previously established transfer method for RPE cells[20], we prepared lentiviral expression constructs for Sema4A^{WT}-FLAG and Sema4A^{F350C}-FLAG. To confirm the expression patterns of these constructs, we transfected 293T cells with each lentiviral construct. As shown in Supplementary Fig. S3, Sema4A^{F350C}-FLAG did not reach the cell surface. Next, the Sema4A^{WT}-FLAG- or Sema4A^{F350C}-FLAG-expressing lentiviral suspension was injected into the subretinal space of 1-week-old *Sema4A*$^{-/-}$ or *Sema4A*$^{F350C/F350C}$ mice using a transvitreous approach (Fig. 6a). Three weeks after injection, the eye tissues were fixed and sectioned. In mice injected with lentiviral vectors expressing Sema4A^{WT}-FLAG, the layer of photoreceptor cells was substantially preserved on the injected side alone in both *Sema4A*$^{-/-}$ and *Sema4A*$^{F350C/F350C}$ retinas (Fig. 6b,c). In contrast, injecting with lentiviral vectors expressing Sema4A^{F350C}-FLAG did not prevent photorecept or degeneration in either *Sema4A*$^{-/-}$ or *Sema4A*$^{F350C/F350C}$ mice. Immunohistochemistry confirmed that the injection of these lentiviral vectors resulted in sustained expression of the Sema4A^{WT}-FLAG or Sema4A^{F350C}-FLAG proteins specifically in RPE cells (Fig. 6b). In addition, injecting lentiviral vectors expressing Sema4A^{WT}-FLAG restored ERG responses to some extent in *Sema4A*$^{-/-}$ and *Sema4A*$^{F350C/F350C}$ retinas (Fig. 6d). Notably, we observed long-term preservation of the photoreceptor layer, lasting at least 4 months after gene transfer (Fig. 7). Thus, we demonstrated a successful means to prevent retinal photoreceptor degeneration using lentivirus-mediated *Sema4A* gene transfer.

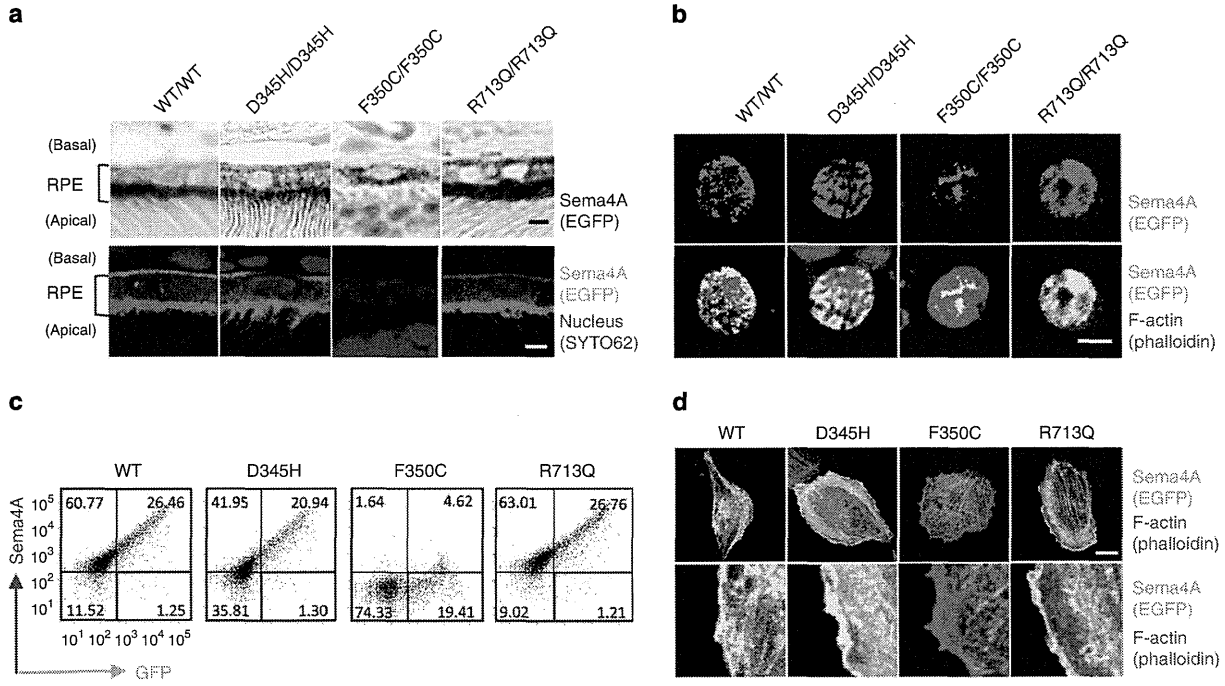

Figure 3 | The Sema4A^{F350C} proteins are mis-localized in RPE cells. (**a**) Representative images of immunostaining of EGFP-tagged Sema4A proteins in RPE cells in *Sema4A$^{WT/WT}$*, *Sema4A$^{D345H/D345H}$*, *Sema4A$^{F350C/F350C}$* and *Sema4A$^{R713Q/R713Q}$* retinas using DAB (top) or fluorescence (bottom). EGFP is shown in brown (top) or green (bottom), and nuclei were visualized with SYTO 62 staining as shown in blue (bottom). Fluorescent signal of EGFP was enhanced by immunostaining using anti-GFP and Alexa Fluor 488-conjugated secondary antibodies (bottom). Scale bar, 2 μm. (**b**) Immunofluorescent images of primary cultured RPE cells derived from *Sema4A$^{WT/WT}$*, *Sema4A$^{D345H/D345H}$*, *Sema4A$^{F350C/F350C}$* and *Sema4A$^{R713Q/R713Q}$* mice. EGFP was stained with anti-GFP and Alexa Fluor 488-conjugated secondary antibodies to enhance the GFP signals (green), and the cytoskeleton was visualized by staining with Alexa Fluor 546-conjugated phalloidin as shown in red. Scale bar, 5 μm. (**c**) Expression of Sema4A on the plasma membrane. COS-7 cells were transfected with plasmid constructs encoding Sema4A^{WT}-EGFP, Sema4A^{D345H}-EGFP, Sema4A^{F350C}-EGFP and Sema4A^{R713Q}-EGFP and incubated for 48 h. Subsequently, the cells were stained with an anti-Sema4A antibody and analysed by flow cytometry. Data are representatives of three experiments. (**d**) ARPE-19 cells were transfected with plasmid constructs expressing Sema4A^{WT}-EGFP, Sema4A^{D345H}-EGFP, Sema4A^{F350C}-EGFP and Sema4A^{R713Q}-EGFP, incubated for 48 h, fixed, stained with Alexa Fluor 546-conjugated phalloidin, and then examined by confocal microscopy. Representative (top) and enlarged images (bottom) are shown. Scale bar, 10 μm.

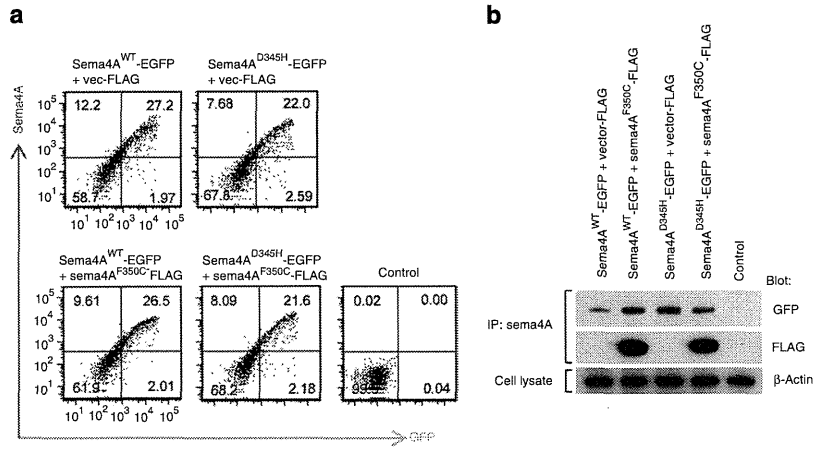

Figure 4 | Sema4A^{F350C} protein does not function in a dominant-negative manner. (**a**) COS-7 cells were transfected with plasmid constructs encoding Sema4A^{WT}-EGFP, Sema4A^{D345H}-EGFP with or without co-transfection of Sema4A^{F350C}-FLAG. After incubation for 48 h, the cells were stained with an anti-Sema4A antibody and analysed by flow cytometry. Control represents untransfected COS-7 cells with staining in the same conditions. (**b**) The same transfected COS-7 cells were lysed and subjected to immunoprecipitation (IP) with an anti-Sema4A antibody and subsequent Western blot analyses using anti-GFP (represents Sema4A^{WT}-EGFP or Sema4A^{D345H}-EGFP) or anti-FLAG (represents Sema4A^{F350C}-FLAG) antibodies. Every Sema4A protein was sufficiently expressed in COS-7 cells.

Discussion

Here we highlighted a novel pathogenic trait of retinal degenerative diseases by analysing a series of knock-in mice with *Sema4A* mutations, which are thought to contribute to human retinal degenerative disease[11]. Among these mice, only *Sema4A*$^{F350C/F350C}$ mice exhibited light-induced retinal degeneration that occurred immediately after birth, which is similar to that observed in *Sema4A*$^{-/-}$ mice (Fig. 2a). In addition, a protein structural modelling and mutational analysis of the Sema4A protein revealed that the side-chain volume of the 350th amino acid is critical for its proper conformation and function in the endosomal sorting of molecules indispensable for

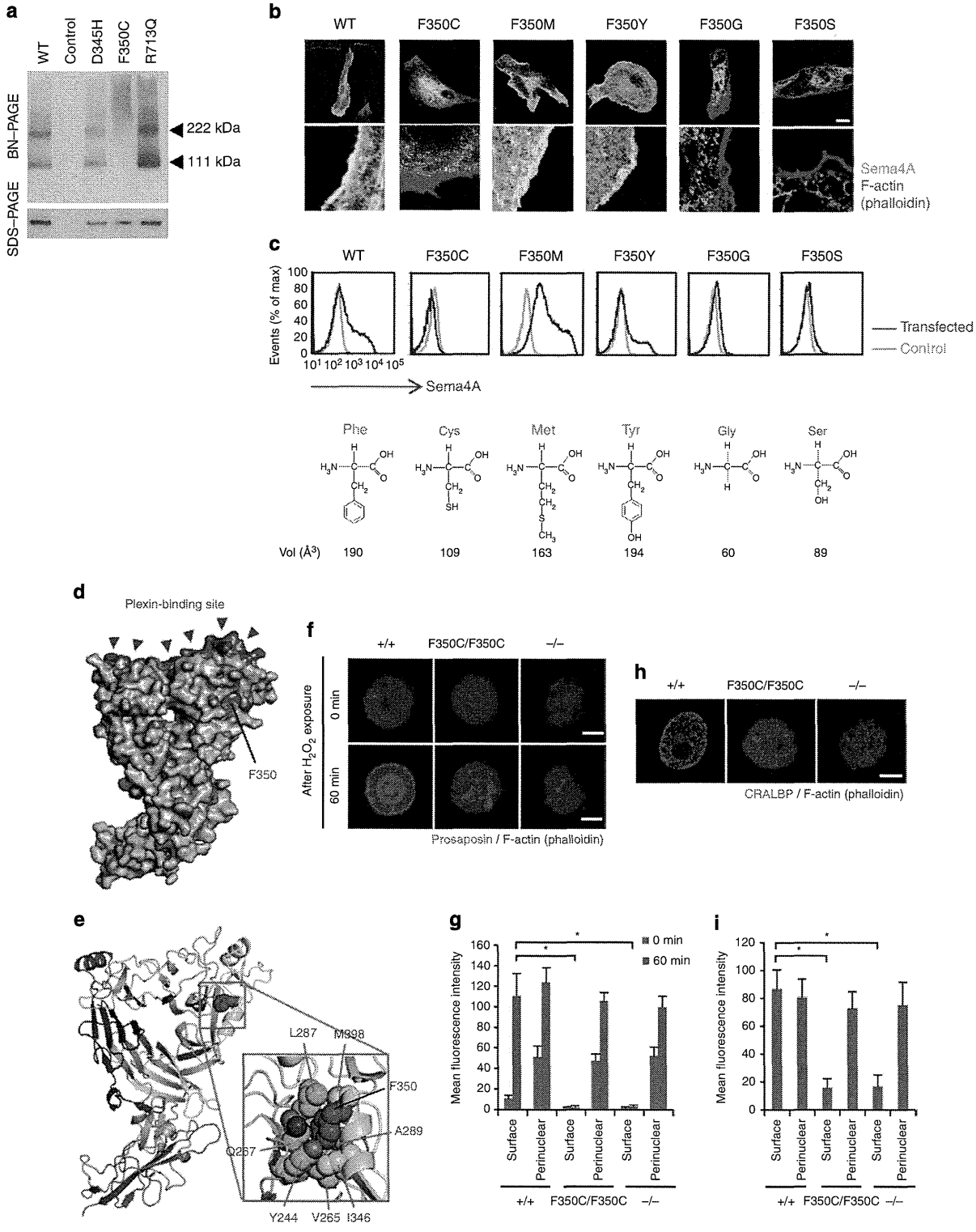

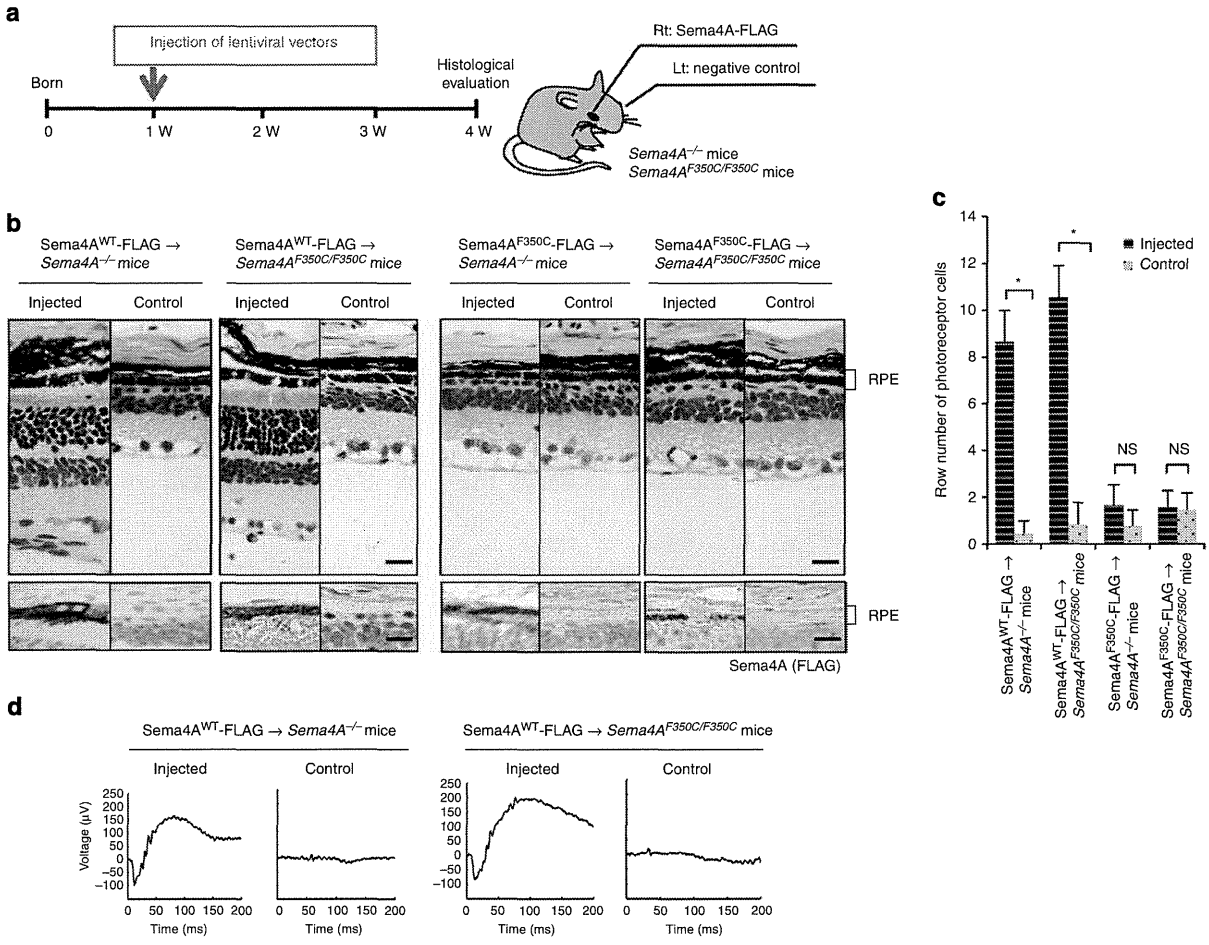

Figure 6 | *Sema4A* gene transfer prevents photoreceptor degeneration in the retinas of *Sema4A*$^{-/-}$ and *Sema4A*$^{F350C/F350C}$ mice. (**a**) Schematic diagram of the protocol: At 1 week of age, suspensions of lentiviral vectors expressing Sema4A^{WT}-FLAG or Sema4A^{F350C}-FLAG were injected into the subretinal space of *Sema4A*$^{-/-}$ or *Sema4A*$^{F350C/F350C}$ infant mice. Viral suspensions were injected into the right eye, while the left eye was used as a negative control (only eyelids were incised). At 4 weeks of age, their eye tissues were fixed and sectioned. (**b**) (Top) Haematoxylin and eosin (HE) staining of the retinal sections from each mouse. Scale bar, 50 μm. (Bottom) The serial sections from those of HE staining were examined by immunohistochemistry (IHC) using an anti-FLAG antibody. Scale bar, 50 μm. (**c**) Histogram showing the average number of photoreceptor cells (± s.e.m.; $n=9$–18) in retinas. *$P<0.01$ (Student's *t*-test); NS, not significant. The number of row of photoreceptor cells was counted at three random points per retinal section in which Sema4A^{WT}-FLAG or Sema4A^{F350C}-FLAG was expressed in immunohistochemistry using an anti-FLAG antibody. (**d**) ERG responses to single flashes were recorded using *Sema4A*$^{-/-}$ or *Sema4A*$^{F350C/F350C}$ mice after *Sema4A* gene transfer. A suspension of lentiviral vectors expressing Sema4A^{WT}-FLAG was injected into the retinas of *Sema4A*$^{-/-}$ or *Sema4A*$^{F350C/F350C}$ mice at 1 week of age, and ERGs were recorded at 4 weeks of age. Viral suspensions were injected into the right eye, while the left eye was used as a negative control (only eyelids were incised).

Figure 5 | The Sema4A^{F350C} proteins exhibit severe structural defects and impaired function. (**a**) BN-PAGE and SDS-PAGE with an anti-Sema4A antibody were performed using cell lysates derived from COS-7 cells transfected with constructs expressing Sema4A-EGFP mutant proteins, or pEGFP vector (negative control). In BN-PAGE, the 222-kDa bands represent Sema4A dimers, while the 111-kDa bands represent Sema4A monomers. SDS-PAGE was performed after immunoprecipitation with an anti-Sema4A antibody, using the same lysate as BN-PAGE. (**b**) Representative images (top) and enlarged images (bottom) obtained by confocal microscopy. ARPE-19 cells were transfected with the plasmid constructs expressing Sema4A^{F350}-EGFP mutant proteins, incubated for 48 h and stained with phalloidin. Scale bar, 10 μm. (**c**) COS-7 cells were transfected with plasmid constructs and incubated for 48 h, stained with an anti-Sema4A antibody and analysed by flow cytometry. Structural diagrams for amino-acid residue replaced with F350 in each mutant are shown below the histograms, together with their apparent volume per molecule in Å^3 (ref. 34). (**d**,**e**) Structural modelling of mouse Sema4A ectodomain, which was built using the structure of human Sema4D structural model previously reported[15]. (**f**) Immunofluorescent images of mouse RPE cells after H_2O_2 treatment (250 μM). Prosaposin (red) was peripherally distributed in wild-type (*Sema4A*$^{+/+}$) RPE cells but not *Sema4A*$^{-/-}$ or *Sema4A*$^{F350C/F350C}$ RPE cells. Scale bar, 5 μm. (**g**) Quantitative analysis of the normalized fluorescence intensity of prosaposin at the surface or perinuclear area of the respective RPE cells with (after 60 min) or without (0 min) H_2O_2 treatment (± s.e.m.; $n=10$). To quantify the intensity, we calculated the mean normalized intensity within the square with its side having an outer 1/6 of radius ('surface') or inner 1/6–3/6 of radius ('perinuclear'). *$P<0.01$ (Student's *t*-test). (**h**) Immunofluorescent images of mouse RPE cells using an anti-CRALBP antibody. Scale bar, 5 μm. (**i**) Quantitative analysis of the normalized fluorescence intensity of CRALBP on the surface or perinuclear area of RPE cells (± s.e.m.; $n=10$–15). *$P<0.01$ (Student's *t*-test).

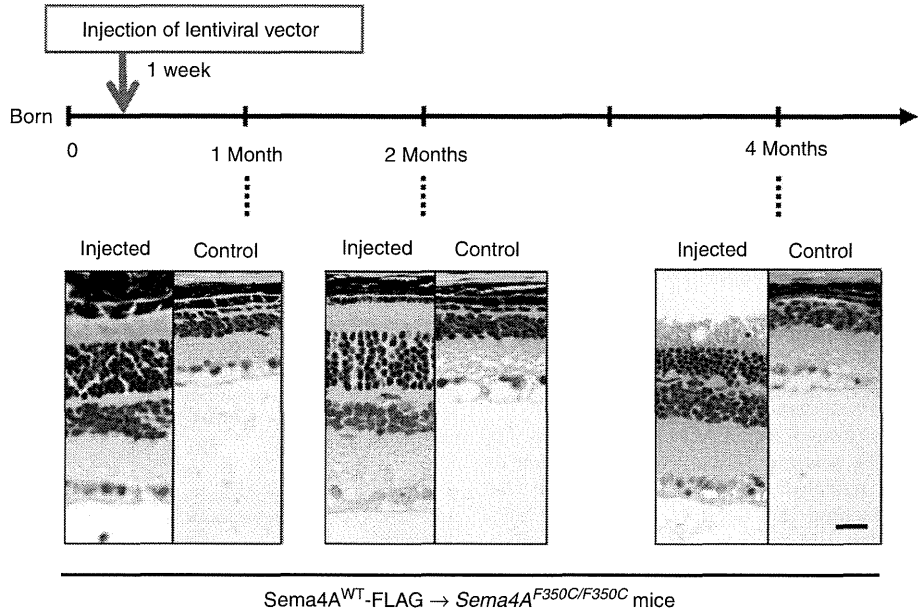

Figure 7 | Long-term prevention of photoreceptor degeneration after *Sema4A* gene transfer. Similar to Figure 6, gene transfer with the lentiviral vectors expressing Sema4A^{WT}-FLAG was performed in 1-week-old Sema4A$^{F350C/F350C}$ mice. Subsequently, we evaluated the retinal histology of these mice at 1, 2 or 4 months of age to estimate the duration of the therapeutic effects. As shown in the representative images, photoreceptor cells were preserved at least 4 months after gene transfer. Scale bar, 50 μm.

photoreceptor survival (Fig. 5d–i). We further determined that *Sema4A* has therapeutic effects in retinal degenerative diseases using virus-mediated gene therapy (Fig. 6).

Recently, we reported that Sema4A mediated the exosomal release of prosaposin and endosomal sorting of retinoid-binding proteins, including CRALBP, in RPE cells[10]. The finding that Sema4A functions as an intracellular guide for specific molecules was highly significant because semaphorins and their receptor plexins were previously shown to function as extracellular guidance molecules[3]. Indeed, our structural modelling of the Sema4A protein indicated that the plexin-binding site is distant from the 350th amino acid (Fig. 5d), suggesting that this mutation does not block this ligand–receptor interaction. This notion is consistent with our previous finding that mice lacking Sema4A receptors exhibited no apparent retinal defects[10]. However, as Plexin-D1-deficient mice die soon after birth[21], we cannot exclude a possibility that the defects are potentially mediated by interacting receptors. Further careful evaluation would be required to determine the pathogenesis.

In addition, BN-PAGE analysis showed that the F350C mutation causes intracellular aggregation of the Sema4A protein, probably within the endoplasmic reticulum, in RPE cells (Fig. 5a). Thus, it appears that this structural defect prevents the protein from being properly transported to its cellular compartments. In this context, the present findings support the notion that Sema4A can function as an 'intracellular navigator' that releases molecules essential for photoreceptor survival. It is also noteworthy that the Sema4A^{F350C} protein did not affect the expression of the Sema4A^{WT} and Sema4A^{D345H} proteins (Fig. 4), indicating that this mutated protein does not function in a dominant-negative manner.

Sema4A$^{D345H/D345H}$ and *Sema4A*$^{R713Q/R713Q}$ mice did not show a disease phenotype in our study (Fig. 2a). In our mouse Sema4A ectodomain model, D345 is located in an α-helix with its side chain well exposed to the solvent and R713 is located in the short cytoplasmic tail region, which is unlikely to form a structural domain. Therefore, both D345H and R713Q do not seem to cause major structural destabilization, which is further supported by the normal cell surface expression of these mutants (Fig. 3a,b). However, we cannot completely exclude the possibility that these mutations contribute to the pathogenicity of human retinal degenerative diseases. There are several possibilities for the differences between our study using mutant mice and a previous human study[11]. First, humans have a longer lifespan than mice, and thus F350C heterozygosity (with D345H) in humans may ultimately induce retinal degenerative disease owing to reduced expression of functional Sema4A proteins. Second, we should carefully evaluate the findings of the human study because this report only sequenced the *Sema4A* gene but did not definitively exclude the possible involvement of other genetic factors. In addition, the human report did not include the phenotypes of F350C homozygotes. Third, slight amino-acid differences between human and mouse Sema4A might contribute to the fragility of the human Sema4A protein structure with a D345H mutation. It has been recently reported that transiently expressed human Sema4A^{D345H} mutant protein showed altered intracellular localization in human RPE cell lines[22]. Additionally, as large-scale sequential analyses of patient DNA have not been performed except for Pakistani individuals[11], further studies will be required to determine whether patients in other racial groups possess the same mutation.

We presented evidence that virus-mediated *Sema4A* gene transfer was successful in an animal model (Fig. 6). Thus, it is theoretically possible to treat this type of retinal degenerative disease with gene therapy, if performed immediately after birth. Recently, considerable progress has been made in the development of gene therapy for retinal degenerative diseases using recombinant adeno-associated virus or lentivirus-based vectors[23]. Currently, *RPE65*, which encodes the retinoid isomerase enzyme and causes Leber congenital amaurosis, is the first and only gene that has been successfully treated by gene transfer therapy in human eyes[24–29]. As *Sema4A* gene transfer displayed a strong

curative effect that was comparable to that of *RPE65* at least in the histology in animal models, it appears that *Sema4A* might be a candidate therapy for retinal degenerative diseases. However, although ERG responses could be detected after gene transfer (Fig. 6d), the levels of responses were relatively low compared to those in WT retinas (Fig. 2b). Deeper investigations would be necessary to reveal the extent of the gene transfer efficacy. As retinal degenerative diseases are caused by many genetic changes, *Sema4A* gene therapy might be limited to a subset of patients carrying *Sema4A* genetic changes, such as the F350C mutation. However, considering the endosomal sorting function of Sema4A for various molecules that are indispensable for retinal homeostasis, it is possible that *Sema4A* replacement gene therapy might be efficacious in a wider subset of patients with retinal degenerative diseases. Further studies are required to assess the potential of *Sema4A* gene therapy.

Collectively, we demonstrated that Sema4A is required for photoreceptor survival. We determined that a point mutation in the *Sema4A* gene causes retinal degenerative disease, which was further supported by structural modelling analyses. The F350C mutation reduces the amino-acid side-chain volume and creates a significant vacant space in the protein interior, which is known to affect the overall stability of the protein[19] and may lead to the precipitation of the protein into non-functional aggregates. Furthermore, photoreceptor degeneration could be rescued by *Sema4A* gene supplementation in an animal model. Our findings provide a novel therapeutic target for retinal degenerative diseases.

Methods

Animals. Sema4A$^{-/-}$ mice (previously established[30]) as well as all knock-in mice (Sema4A$^{WT/WT}$ mice, Sema4A$^{D345H/D345H}$ mice, Sema4A$^{F350C/F350C}$ mice, Sema4A$^{R713Q/R713Q}$ mice, Sema4A$^{D345H/F350C}$ mice, Sema4A$^{WT/+}$ mice, Sema4A$^{D345H/+}$ mice, Sema4A$^{F350C/+}$ mice and Sema4A$^{R713Q/+}$ mice) and WT mice (Sema4A$^{+/+}$ mice) with the same genetic background (C57BL/6J) were housed under a 12-h light/12-h dark cycle (60 lux at the cage level). All animal procedures were performed in accordance with institutional guidelines.

Construction of the expression vector and site-directed mutagenesis. The cDNA sequence encoding full-length *Sema4A* (amino acids 1–760) was generated by PCR and then ligated into pEGFP-N3 (Clontech, Palo Alto, CA) or p3xFLAG-CMV-14 (Sigma-Aldrich Co., Milwaukee, WI). Various mutant constructs (Sema4A^{D345H}-EGFP, Sema4A^{F350C}-EGFP, Sema4A^{R713Q}-EGFP, Sema4A^{F350M}-EGFP, Sema4A^{F350Y}-EGFP, Sema4A^{F350G}-EGFP, Sema4A^{F350S}-EGFP and Sema4A^{F350C}-FLAG) were generated from Sema4A^{WT}-EGFP or Sema4A^{WT}-FLAG using a QuikChange II XL site-directed mutagenesis kit (Stratagene, La Jolla, CA) according to the manufacturer's protocol.

Gene targeting strategy. DNA fragments were isolated from Sema4A^{WT}-EGFP, Sema4A^{D345H}-EGFP, Sema4A^{F350C}-EGFP and Sema4A^{R713Q}-EGFP constructs. To construct targeting vectors (for *Sema4A$^{WT/WT}$*, *Sema4A$^{D345H/D345H}$*, *Sema4A$^{F350C/F350C}$* and *Sema4A$^{R713Q/R713Q}$* mice), the 3.1-kb fragments encoding full-length WT or mutant *Sema4A* cDNA containing EGFP at the C-terminus were placed into exon 2 and exon 3 in the intact Sema4A alleles. The Herpes simplex virus thymidine kinase (*HSV-tk*) gene was inserted to select against random integration. The linearized targeting plasmid DNA was electroporated into ES cells. After selecting with G418, resistant colonies were screened for homologous recombination of the *Sema4A*-targeted allele by PCR and Southern blot analysis. The clones with homologous recombination were identified and isolated. These ES cells were injected into blastocysts from C57BL/6J mice. The blastocysts were transferred to pseudopregnant ICR foster mothers, and chimeric males were obtained. Subsequently, chimeric males and WT females were mated to produce heterozygous, targeted mice.

Cell culture. ARPE-19 cells, COS-7 cells and 293T cells were grown in DMEM supplemented with 10% fetal calf serum. RPE cells were isolated from 10-day-old mice for primary cultures following an experimental procedure that was previously described[31]. Briefly, enucleated eyecups were treated with 2% dispase (Invitrogen, San Diego, CA) and 0.5% trypsin/EDTA (Gibco BRL Life Technologies, Rockville, MD), and the isolated RPE cells were seeded into fibronectin-coated cell culture dishes (BD BioCoat) (BD Bioscience, San Jose, CA) and grown in DMEM containing 10% fetal bovine serum at 37 °C. RPE cells were successfully subcultured using 0.5% trypsin/EDTA every 7 days for 1 month.

Immunomethods. The antibodies used to detect Sema4A were previously described[30]. The other antibodies used in this study include anti-GFP (Cell Signaling Technology Inc., Danvers, MA), anti-FLAG (Cell Signaling Technology Inc., Danvers, MA), anti-prosaposin (Abcam, Cambridge, UK) and anti-CRALBP (Abcam, Cambridge, UK). Cells were transfected using FuGENE HD (Roche Applied Science, Indianapolis, IN) and then incubated for 2 days, collected and lysed in lysis buffer (50 mM Tris–HCl at pH 8.0, 250 mM NaCl, 5 mM EDTA, 1% NP-40, 0.25% Na-deoxycholate and 1 mM NaF) for immunoprecipitation and immunoblot analyses, which were performed using standard protocols.

SDS-polyacrylamide gel electrophoresis (SDS-PAGE) and BN-PAGE. For SDS–PAGE, samples were boiled for 5 min in SDS–PAGE sample buffer containing 0.125 mM Tris–HCl, pH 6.8, 20% glycerol, 4% SDS, 10% 2-mercaptoethanol and 0.004% bromophenol blue. The protein samples were loaded onto NuPAGE 4–12% Bis–Tris gels (Invitrogen, San Diego, CA). BN-PAGE systems were purchased from Invitrogen, and sample preparation and electrophoresis were performed according to the manufacturer's instructions. For immunoblot analysis, the gel was electroblotted onto a PVDF membrane, which was blocked in 5% skim milk and incubated with an anti-Sema4A antibody followed by a goat anti-rabbit secondary antibody.

Immunohistochemistry of paraffin-embedded specimens. Eyecup specimens were fixed in 4% paraformaldehyde and routinely processed for paraffin embedding. Paraffin-embedded specimens were cut into 4-μm-thick sections and stained using the immunoperoxidase procedure. After antigen retrieval with a Pascal pressurized heating chamber (DAKO A/S, Glostrup, Denmark), the sections were treated with Melanin bleach Kit (Polysciences Inc., Warrington, PA) to remove melanin from RPE cells, incubated with the indicated antibodies and then treated with ChemMate EnVision kit (DAKO A/S, Glostrup, Denmark). DAB (DAKO A/S, Glostrup, Denmark) was used as a chromogen.

Immunohistochemistry of frozen specimens. Frozen sections of 4% paraformaldehyde-fixed eyecups of 8 μm thickness were prepared. The sections were treated with Melanin bleach Kit (Polysciences Inc., Warrington, PA) to remove melanin from RPE cells, incubated with a blocking solution (5% BSA in PBS containing 0.5% Triton X-100) for 1 h, and then stained overnight with the indicated antibodies. Confocal images were obtained using an LSM 5 EXCITER (Ver 4.2) confocal inverted microscope (Carl Zeiss MicroImaging, Jena, Germany).

TUNEL assay. TUNEL assay systems (DeadEnd Fluorometric TUNEL system) were purchased from Promega (Madison, WI). Prepared frozen sections were processed according to the manufacturer's protocol. Sections were imaged using an LSM 5 EXCITER (Ver 4.2) confocal inverted microscope (Carl Zeiss MicroImaging, Jena, Germany).

Electroretinography. Conventional full-field ERGs were recorded *in vivo* using a PuREC system with two built-in white LED contact lens electrodes (Mayo, Aichi, Japan). Mice were dark-adapted overnight and all subsequent procedures were performed under dim red light. Before the ERG recordings, mice were anaesthetized and placed on a heating pad held at 37 °C throughout the experiments. The pupils were dilated with a cocktail of 0.05% tropicamide and 0.05% phenylephrine hydrochloride. 0.5% hydroxyethyl cellulose was applied to the eyes to maintain corneal hydration. Needle electrodes placed subcutaneously in the forehead and tail served as reference and ground electrode, respectively. Single-flash recordings were performed at a light intensity of 2.0 log cd s m^{-2} using a sampling frequency of 1,253 Hz and a flash duration of 13.3 ms. The band-pass filter was set between 0.3 and 500 Hz. In addition, the obtained data were low-pass filtered at 300 Hz using a PuREC software (Mayo, Aichi, Japan).

Homology model building. Sequence alignments of the ectodomain portions of mouse Sema4A (residues 36–650) and human Sema4D (residues 24–648) were generated using CLUSTALW[32]. Homology model building was performed with the programme MODELLER[33] using the human Sema4D ectodomain structure (PDB ID: 1OLZ)[15] as a template.

Preparation of lentiviral vectors. C-terminal FLAG-tagged *Sema4A* cDNA fragments with or without the F350C mutation were isolated and amplified by PCR from the Sema4A^{WT}-p3xFLAG-CMV-14 or Sema4A^{F350C}- p3xFLAG-CMV-14 constructs. The PCR primers contained an *AgeI* site at the 5′-terminus and *EcoRI* site at the 3′-terminus. Primer sequences are described in Supplementary Table S1. This fragment was digested with *AgeI* and *EcoRI*, and subsequently subcloned into the *AgeI* and *EcoRI* sites of CSII-CMV-MCS (RIKEN, Tokyo, Japan). The titres of the Sema4A^{WT}-FLAG and Sema4A^{F350C}-FLAG lentiviral vectors were determined by quantitative RT-PCR using viral RNA from 293T cells infected with these vectors. After the virus was concentrated by ultracentrifugation, titres of 5×10^7 infectious units ml^{-1} for the Sema4A^{WT}-FLAG lentiviral vector and

1.3×10^7 infectious units ml^{-1} for the Sema4A^{F350C}-FLAG lentiviral vector were obtained.

***In vivo* delivery of lentiviral vectors**. Infant mice (1 week of age) were anaesthetized. The eyeball was exposed by an incision in the eyelid, parallel to the future edge of the open eyelid. Subretinal injections were performed under an operating microscope. A small incision was made in the sclera, and 2 µl of undiluted vector suspension (titres of $1.3–5 \times 10^7$ infection units ml^{-1} on 293T cells) was injected through the incision into the subretinal space using a glass capillary connected to a 10-µl syringe.

References

1. Pacione, L. R. *et al.* Progress toward understanding the genetic and biochemical mechanisms of inherited photoreceptor degenerations. *Annu. Rev. Neurosci.* **26,** 657–700 (2003).
2. Wright, A. F. *et al.* Photoreceptor degeneration: genetic and mechanistic dissection of a complex trait. *Nat. Rev. Genet.* **11,** 273–284 (2010).
3. Kolodkin, A. L., Matthes, D. J. & Goodman, C. S. The semaphorin genes encode a family of transmembrane and secreted growth cone guidance molecules. *Cell* **75,** 1389–1399 (1993).
4. Serini, G. *et al.* Class 3 semaphorins control vascular morphogenesis by inhibiting integrin function. *Nature* **424,** 391–397 (2003).
5. Neufeld, G. & Kessler, O. The semaphorins: versatile regulators of tumour progression and tumour angiogenesis. *Nat. Rev. Cancer* **8,** 632–645 (2008).
6. Toyofuku, T. *et al.* Dual roles of Sema6D in cardiac morphogenesis through region-specific association of its receptor, Plexin-A1, with off-track and vascular endothelial growth factor receptor type 2. *Genes Dev.* **18,** 435–447 (2004).
7. Suzuki, K., Kumanogoh, A. & Kikutani, H. Semaphorins and their receptors in immune cell interactions. *Nat. Immunol.* **9,** 17–23 (2008).
8. Takamatsu, H. & Kumanogoh, A. Diverse roles for semaphorin-plexin signaling in the immune system. *Trends Immunol.* **33,** 127–135 (2012).
9. Rice, D. S. *et al.* Severe retinal degeneration associated with disruption of Semaphorin 4A. *Invest. Ophthalmol. Vis. Sci.* **45,** 2767–2777 (2004).
10. Toyofuku, T. *et al.* Endosomal sorting by Semaphorin 4A in retinal pigment epithelium supports photoreceptor survival. *Genes Dev.* **26,** 816–829 (2012).
11. Abid, A. *et al.* Identification of novel mutations in the SEMA4A gene associated with retinal degenerative diseases. *J. Med. Genet.* **43,** 378–381 (2006).
12. Lamb, T. D. & Pugh, Jr. E. N. Dark adaptation and the retinoid cycle of vision. *Prog. Retin. Eye Res.* **2,** 307–380 (2004).
13. Schägger, H. & von Jagow, G. Blue native electrophoresis for isolation of membrane protein complexes in enzymatically active form. *Anal. Biochem.* **199,** 223–231 (1991).
14. Antipenko, A. *et al.* Structure of the semaphorin-3A receptor binding module. *Neuron* **39,** 589–598 (2003).
15. Love, C. A. *et al.* The ligand-binding face of the semaphorins revealed by the high-resolution crystal structure of SEMA4D. *Nat. Struct. Biol.* **10,** 843–848 (2003).
16. Janssen, B. J. *et al.* Structural basis of semaphorin–plexin signaling. *Nature* **467,** 1118–1122 (2010).
17. Nogi, T. *et al.* Structural basis for semaphorin signalling through the plexin receptor. *Nature* **467,** 1123–1127 (2010).
18. Liu, H. *et al.* Structural basis of semaphorin-plexin recognition and viral mimicry from Sema7A and A39R complexes with PlexinC1. *Cell* **142,** 749–761 (2010).
19. Atwell, S., Ultsch, M., De Vos, A. M. & Wells, J. A. Structural plasticity in a remodeled protein-protein interface. *Science* **278,** 1125–1128 (1997).
20. Miyoshi, H., Takahashi, M., Gage, F. H. & Verma, I. M. Stable and efficient gene transfer into the retina using an HIV-based lentiviral vector. *Proc. Natl Acad. Sci. USA* **94,** 10319–10323 (1997).
21. Gitler, A. D., Lu, M. M. & Epstein, J. A. PlexinD1 and semaphorin signaling are required in endothelial cells for cardiovascular development. *Dev. Cell* **7,** 107–116 (2004).
22. Tsuruma, K. *et al.* SEMA4A mutations lead to susceptibility to light irradiation, oxidative stress, and ER stress in retinal pigment epithelial cells. *Invest. Ophthalmol. Vis. Sci.* **53,** 6729–6737 (2012).
23. Bainbridge, J. W., Tan, M. H. & Ali, R. R. Gene therapy progress and prospects: the eye. *Gene Ther.* **13,** 1191–1197 (2006).
24. Van Hooser, J. P. *et al.* Rapid restoration of visual pigment and function with oral retinoid in a mouse model of childhood blindness. *Proc. Natl Acad. Sci. USA* **97,** 8623–8628 (2000).
25. Acland, G. M. *et al.* Gene therapy restores vision in a canine model of childhood blindness. *Nat. Genet.* **28,** 92–95 (2001).
26. Jacobson, S. G. *et al.* Identifying photoreceptors in blind eyes caused by RPE65 mutations: prerequisite for human gene therapy success. *Proc. Natl Acad. Sci. USA* **102,** 6177–6182 (2005).
27. Bainbridge, J. W. *et al.* Effect of gene therapy on visual function in Leber's congenital amaurosis. *N. Engl. J. Med.* **358,** 2231–2239 (2008).
28. Maguire, A. M. *et al.* Safety and efficacy of gene transfer for Leber's congenital amaurosis. *N. Engl. J. Med.* **358,** 2240–2248 (2008).
29. Maguire, A. M. *et al.* Age-dependent effects of RPE65 gene therapy for Leber's congenital amaurosis: a phase 1 dose-escalation trial. *Lancet* **374,** 1597–1605 (2009).
30. Kumanogoh, A. *et al.* Nonredundant roles of Sema4A in the immune system: defective T cell priming and Th1/Th2 regulation in Sema4A-deficient mice. *Immunity* **22,** 305–316 (2005).
31. Geisen, P. *et al.* Characterization of barrier properties and inducible VEGF expression of several types of retinal pigment epithelium in medium-term culture. *Curr. Eye Res.* **31,** 739–748 (2006).
32. Larkin, M. A. *et al.* Clustal W and Clustal X version 2.0. *Bioinformatics* **23,** 2947–2948 (2007).
33. Eswar, N. *et al.* Protein structure modeling with MODELLER. *Methods Mol. Biol.* **426,** 145–159 (2008).
34. Zamyatnin, A. A. Protein volume in solution. *Prog. Biophys. Mol. Biol.* **24,** 107–123 (1972).

Acknowledgements

This study was supported by research grants from the Ministry of Education, Culture, Sports, Science, and Technology of Japan (T.T. and A.K.); Funding Programme for Next-Generation World-Leading Researchers (NEXT Program); and CREST (A.K.).

Author contributions

S.N. and T.T. carried out most of the *in vivo* and *in vitro* experiments. H.K. and C.I. performed the virus-mediated gene transfer experiment, J.K. performed ERGs, and M.T. designed and supervised these experiments. J.T. built a structural model and contributed to manuscript preparation. M.I. and D.I. supported breeding of animals. E.M. and K.A. conducted histopathological analysis. T.O., H.T., D.I., S.K., T.K., Y.Y., K.M., Y.M. and A.O. contributed to preparation of materials and provided advice on project planning and data interpretation. T.T. and A.K. designed and supervised the project, and wrote the manuscript.

Additional information

Supplementary Information accompanies this paper at http://www.nature.com/naturecommunications

Competing financial interests: The authors declare no competing financial interests.

Reprints and permission information is available online at http://npg.nature.com/reprintsandpermissions/

How to cite this article: Nojima, S. *et al.* A point mutation in *Semaphorin 4A* associates with defective endosomal sorting and causes retinal degeneration. *Nat. Commun.* 4:1406 doi: 10.1038/ncomms2420 (2013).

Clinical Medicine Insights: Therapeutics

REVIEW

Tocilizumab: An Updated Review of Its Use in the Treatment of Rheumatoid Arthritis and Its Application for Other Immune-Mediated Diseases

Toshio Tanaka[1,2], Atsushi Ogata[2,3] and Masashi Narazaki[3]

[1]Department of Clinical Application of Biologics, Osaka University of Graduate School of Medicine, Osaka University, [2]Department of Immunopathology, WPI Immunology Frontier Research Center, Osaka University, [3]Department of Respiratory Medicine, Allergy and Rheumatic Diseases, Osaka University Graduate School of Medicine, Osaka University, Osaka, Japan. Corresponding author email: ttanak@imed3.med.osaka-u.ac.jp

Abstract: Interleukin-6 (IL-6), produced by a variety of cells, is a typical cytokine featuring redundancy and pleiotropic activity. IL-6 is promptly and transiently synthesized in response to infections or injuries, and participates in host defense by inducing immune responses, hematopoiesis, and acute-phase reactions. However, since its abnormal persistent production of mostly unknown etiology plays an important pathological role in the development of various immune-mediated diseases, a humanized anti-IL-6 receptor monoclonal antibody, tocilizumab, was developed and is now used as an innovative biologic for rheumatoid arthritis in more than 90 countries. Several factors strongly suggest that a IL-6 blockade strategy may have a broad application for the treatment of various immune-mediated diseases. These factors include favorable results of pilot or case studies with off-label use of tocilizumab, pathological analyses of the contribution of IL-6 to the development of immune-mediated diseases, and the potential capability of tocilizumab to both repair an imbalance of effector T cell subsets and to suppress pathologic autoantibody production. However, clinical trials to evaluate the efficacy and safety of tocilizumab for these diseases are essential. Furthermore, clarification of the cell source of IL-6 production and of the mechanisms through which dysregulated continuous IL-6 synthesis is induced constitutes an important issue for future studies into the pathogenesis of diseases.

Keywords: anti-IL-6 receptor antibody, IL-6, immune-mediated diseases, rheumatoid arthritis, tocilizumab

Clinical Medicine Insights: Therapeutics 2013:5 33–52

doi: 10.4137/CMT.S9282

This article is available from http://www.la-press.com.

Interleukin-6

In the early stages of research into the soluble factor interleukin-6 (IL-6), its various and distinct functions were being studied and each research group had its own name for this cytokine. One was B cell stimulatory factor 2 (BSF-2) because it induces B-cell differentiation into antibody (Ab) producing cells. Another was hepatocyte-stimulating factor (HSF) because it induces synthesis of acute phase proteins in hepatocytes. Yet another was hybridoma growth factor (HGF) due to its promotion of growth of fusion cells with myeloma, or IFNβ2 due to its IFN anti-viral activity. Later, it was discovered that these diverse functions reflect the wide range of target organs for IL-6.[1] In 1986, two groups independently reported on the molecular structures of IFNβ2 and BSF-2.[2,3] Since these two molecules were found to be identical, the cytokine was renamed IL-6. Human IL-6 (GenBank: X04602) consists of 212 amino acids, includes a 28-amino-acid signal peptide, and its gene has been mapped to chromosome 7p21. The structure of IL-6 includes four helix bundles, which are arranged in an up-up-down-down topology (Fig. 1: A to D), and three loops (two long ones, A–B and C–D, and a short one, B–C).[4]

IL-6 mediates inflammatory signals from infected or injured lesions to other parts of the body in order to generate protection against emergent events. There are many cytokines that are involved in and regulate inflammation, but IL-6 is the most imoprtant for mediating systemic inflammation. The clinical function of IL-6 was discovered first by observing and examining patients with cardiac myxoma or Castleman's disease in whom IL-6 was persistently produced from myxoma tissues or involved lymph nodes, respectively.[5,6] These patients presented with symptoms of systemic inflammation and autoimmunity (eg, fever, arthralgia, fatigue) and laboratory findings of inflammation such as elevated C-reative protein (CRP), serum amyloid A (SAA), and fibrinogen levels, as well as thrombocytosis. As a result of chronic inflammation, anemia, autoantibody production, hypergammaglobulinemia and hypoalbuminemia were also detected. The fact that all of these signs and laboratory data became normalized after surgical removal of cardiac myxoma suggested that IL-6 played a role in systemic inflammation. An IL-6 deficient mouse model was thus compared with its IL-6 transgenic expression counterpart. The IL-6 deficient mice could develop almost normally and were fertile,[7] indicating that IL-6 is not essential for organ development, whereas mice with persistent IL-6 expression showed chronic inflammation accompanied by swollen lymph nodes and spleen.[8] Similarly, healthy human individuals feature almost undetectable serum IL-6 levels, whereas in those with infection, trauma or burn IL-6 levels increase and inflammatory symptoms appear.[9] These findings indicate that production of IL-6 provides an SOS signal to indicate occurrence of an emergent infection or injury in an organ.

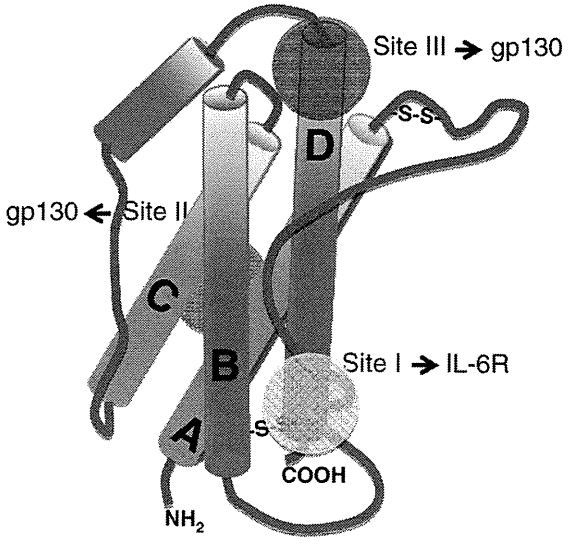

Figure 1. Schematic representation of the domain structure of human IL-6.
Notes: The human IL-6 structure consists of the four long α-helices, A–D, and three connecting loops. Two disulfide bonds are contained in loop (A and B). Site I on the C-terminal end of helix D interacts with IL-6 receptor (IL-6R); site II, located on helices A and C, interacts with one gp130; and site III on the N-terminal end of helix D interacts with another gp130.

In infectious stress, IL-6 is promptly produced by monocytes and macrophages through the stimulation of Toll-like receptors (TLRs) by microbial motifs.[10] IL-6, when acting on hepatocytes, induces a wide spectrum of acute phase proteins, such as CRP, SAA, fibrinogen, and hepcidin, and inhibits the synthesis of albumin (Fig. 2).[11] High levels of hepcidin cause increased internalisation of iron transporter ferroportin molecules on cell membranes, which inhibits release from iron stores and leads to anemia of chronic disease.[12] Induction of zinc transporter Zip14 by IL-6 in liver increases zinc uptake into hepatocytes, resulting in hypozincemia.[13] IL-6 in the bone marrow promotes maturation of megakaryocytes, which leads to the production of platelets.[14] These changes

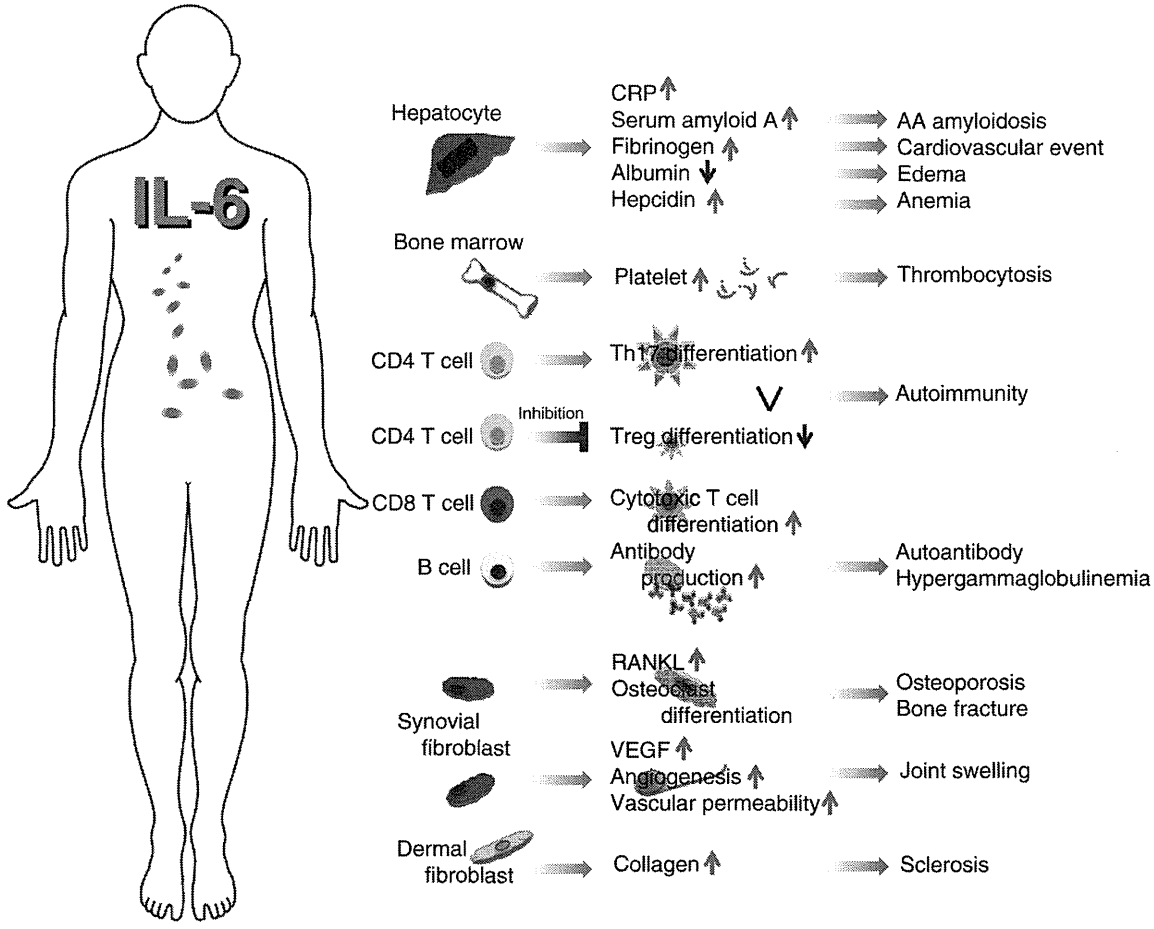

Figure 2. Pleiotropic activity of IL-6.
Notes: IL-6 induces cell differentiation and specific gene expression. It also induces production of acute-phase proteins such as CRP, serum amyloid A, fibrinogen, and hepcidin. On the other hand, it reduces synthesis of albumin in hepatocytes. In bone marrow, IL-6 induces maturation of megakaryocytes into platelets. In addition, IL-6 together with TGF-β promotes Th17 differentiation from naïve CD4 T cells, whereas it inhibits TGF-β-induced Treg differentiation. IL-6 promotes immunoglobulin synthesis in activated B cells. IL-6 also acts on synovial fibroblasts to produce RANKL and VEGF, which promote differentiation of osteoclasts and angiogenesis, respectively. Furthermore, IL-6 stimulates dermal fibroblasts to produce collagen.
Abbreviations: CRP, C-reactive protein; Treg, regulatory T cells; RANKL, receptor activator of NF-κB ligand; VEGF, vascular endothelial growth factor.

in acute phase serum protein levels and red blood cell and platelet counts are in fact used in clinical practice for the diagnosis and evaluation of inflammatory severity. After the infiltration of neutrophils into the focus of acute infection, IL-6 orchestrates the switch in leukocyte recruitment from neutrophils to more sustained monocytic cells that develop acquired immune responses.[15] IL-6 thus performs an important function in acquired immunity. In lymphocytes, CD4-positive T-helper cells display distinct effector functions after their differentiation.[16] IL-6, together with TGF-β, has been shown to be essential for Th17 differentiation from naive CD4-positive T cells.[17] On the other hand, IL-6 inhibits the generation of regulatory T cells (Treg) induced by TGF-β.[16,17] The resultant Th17/Treg imbalance leads to a rupture in immunological tolerance and is thus essential for the development of autoimmune or chronic inflammatory diseases.[18] IL-6 also acts on CD8-positive T cells to induce cytotoxic T cells,[19] and on activated B cells for differentiation into Ab producing cells.[20] Besides its effects on hepatocytes and lymphocytes, IL-6 has various effects that are associated with inflammatory symptoms. For example, IL-6 production in bone marrow stromal cells induces the receptor activator of NF-kappaB ligand (RANKL), which is an essential factor for the differentiation and activation of osteoclasts and bone resorption.[21,22] IL-6 production by bone marrow stromal cells is

suppressed by 17 beta-estradiol and in mice the loss of estrogen due to ovariectomy increased the number of osteoclasts in trabecular bone. Conversely, the administration of 17 beta-estradiol or anti-IL-6 Ab prevented such an increase,[23] suggesting that estrogen loss results in an IL-6-mediated bone resorption in postmenopausal osteoporosis and affects the development of rheumatoid arthritis (RA) in postmenopausal women.[24] Furthermore, enhanced angiogenesis and increased vascular permeability are pathological features of chronic inflammatory sites such as synovial tissue of RA; these pathological changes are due to the excess production of vascular endothelial growth factor (VEGF), which is induced by IL-6.[25] Finally, IL-6 has been demonstrated to promote the proliferation of keratinocytes[26] and collagen production[27] in dermal fibroblasts.

The IL-6 receptor (IL-6R) system consists of two chains, IL-6-binding chain IL-6R and gp130, both of which belong to the cytokine receptor family.[28] The latter transduces the IL-6 signal into cells.[29] The broad range of expression of gp130 on various cells suggests that IL-6 has pleiotropic effects because the soluble form of IL-6R (sIL-6R) is present in human serum.[30] The IL-6/sIL-6R complex can transduce the IL-6 signal on gp130-expressing cells even in cells lacking transmembrane IL-6R. The IL-6/IL-6R complex in turn induces homodimerization of gp130 to trigger downstream events in cytoplasm (Fig. 3). The activated IL-6 receptor complex is formed as a hexameric structure comprising two molecules each of IL-6, IL-6R, and gp130.[31] In this complex, IL-6 provides one IL-6R binding site (site I) and two gp130 binding sites (sites II and III) (Fig. 1). IL-6R is a unique binding receptor for IL-6 and its expression is restricted to certain cells, including leukocytes and hepatocytes, whereas signal-transducing chain gp130 is expressed in almost all cells and is shared by members of the IL-6 family of cytokines.[32] These members include leukemia inhibitory factor (LIF), oncostatin M (OSM), ciliary neurotrophic factor (CNTF), IL-11, cardiotrophin 1 (CTF1), cardiotrophin-like cytokine (CLC), IL-27, and IL-35.[33] These cytokines bind to their unique binding receptors but use their common gp130 to transduce their signal. The only exception is virus-encoded IL-6 (vIL-6), which is the product of Kaposi's sarcoma-associated herpes virus (also known as human herpes virus 8) and directly binds to

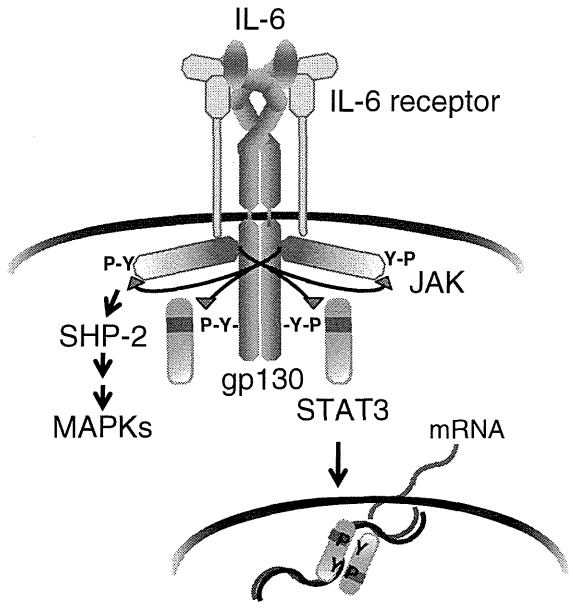

Figure 3. IL-6 receptor system.
Notes: After binding of IL-6 to IL-6 receptor (IL-6R), the resultant IL-6/IL-6R complex associates with gp130 and induces homodimerization of gp130; this in turn triggers activation of JAKs and tyrosine phosphorylation of gp130. The phosphorylated gp130 then recruits STAT3 via the SH2-domain. Next, activated STAT3 translocates into the nucleus and regulates transcription for various sets of genes. Tyrosine-phosphorylated gp130 also recruits SHP-2 and activates the MAP kinase pathway.
Abbreviations: JAKs, Janus kinase family tyrosine kinases; STAT3, signal transducer and activator of transcription 3; SHP-2, SH2-domain containing protein tyrosine phosphatase-2; MAPK, mitogen-activated protein kinase.

and activates gp130.[34] It is known that the activities of the IL-6 family of cytokines often overlap with those of IL-6. The model in which IL-6 family members use the common signal-transducing chain makes it clear why different cytokines show functional redundancy. Activated gp130 triggers activation of the JAK (Janus kinase)-STAT3 (signal transducer and activator of transcription 3) pathway and the JAK-SH2-domain containing protein tyrosine phosphatase-2 (SHP-2)-mitogen-activated protein (MAP) kinase pathway. In this context, STAT3 is the transcriptional factor that regulates various sets of IL-6 responsive genes, including acute phase proteins.[28]

IL-6 is produced from inflammatory lesions. The synthesis of IL-6 is strictly regulated both through levels of gene transcription and the stability of mRNA. The transcriptional factors NF-kB and NF-IL-6 (also known as C/EBPβ) promote transcription of IL-6 mRNA in response to various stimuli.[35,36] Some RNA binding proteins or micro-RNAs bind to the 3′-untranslated regions of the IL-6 mRNA so as